Surface impedance and topologically protected interface modes in one-dimensional phononic crystals

Antonin Coutant, Bruno Lombard

Surface impedance and topologically protected interface modes in one-dimensional phononic crystals

Antonin Coutant[a], Bruno Lombard[a,*]

[a] *Aix Marseille Univ, CNRS, Centrale Marseille, LMA UMR 7031, Marseille, France*

Abstract

When semi-infinite phononic crystals (PCs) are in contact, localized modes may exist at their boundary. The central question is generally to predict their existence and to determine their stability. With the rapid expansion of the field of topological insulators, powerful tools have been developed to address these questions. In particular, when applied to one-dimensional systems with mirror symmetry, the bulk-boundary correspondence claims that the existence of interface modes is given by a topological invariant computed from the bulk properties of the phononic crystal, which ensures strong stability properties. This one-dimensional bulk-boundary correspondence has been proven in various works. Recent attempts have exploited the notion of surface impedance, relying on analytical calculations of the transfer matrix. In the present work, the monotonic evolution of surface impedance with frequency is proven for all one-dimensional phononic crystals with mirror symmetry. This result allows us to establish a stronger version of the bulk-boundary correspondence that guarantees not only the existence but also the uniqueness of a topologically protected interface state. This correspondence is extended to a larger class of one-dimensional models that include imperfect interfaces, array of resonators, or dispersive media. Numerical simulations are proposed to illustrate the theoretical findings.

Keywords: periodic media, linear waves, imperfect interfaces, Bloch-Floquet theory, inversion symmetry, Zak phase.

Contents

1 Introduction **1**

2 Problem statement **3**

2.1 Physical modeling 3

2.2 Band structure 3

*Corresponding author. Tel.: +33 491 84 52 42 53.

Email addresses: coutant@lma.cnrs-mrs.fr (Antonin Coutant), lombard@lma.cnrs-mrs.fr (Bruno Lombard)

3 Phononic crystals with mirror symmetry **4**
3.1 Parity of Bloch modes 4
3.2 Change of parity across a gap 6
3.3 Relation between Zak phase and Bloch mode symmetry 7

4 Semi-infinite phononic crystals **8**
4.1 Surface impedance 8
4.2 Monotony of the surface impedances in gaps 9
4.3 Topologically protected interface mode 11
4.4 Absence of edge mode for one-sided systems 11
4.5 Numerical example: the bilayer model 12

5 Generalizations **16**
5.1 Framework 16
5.2 Bulk-boundary correspondence for a generalized Helmholtz equation 17
5.3 Families of models 19
5.4 Numerical example: array of imperfect contacts 20

6 Conclusion **26**

Appendix A Zak phase as a topological invariant **27**

Appendix B Transfer matrix **28**

Appendix C Jump of the Wronskian across an imperfect interface **30**

1. Introduction

Periodic media have forbidden frequency bands, in which waves cannot propagate. This property is very much used in various fields of wave physics, from quantum mechanics [1] to electromagnetism [2] or acoustics [3]. It has been the subject of a great deal of theoretical work, particularly in spectral theory [4]. When two phononic/photonic crystals (PCs) are joined, interface modes can exist in the gaps common to both crystals, depending on the coupling between the media [5]. These modes then remain localized (in one dimension (1D)) or can propagate at the interface (in 2D or more). However, their stability is not guaranteed. In the presence of manufacturing defects or impurities, these waves are then diffracted in all directions, losing the benefit of guidance.

Recently, the notion of *topological insulators*, initially discovered in the context of the quantum Hall effect, has provided a powerful approach to obtain localized modes with high robustness against defects [6, 7]. If certain symmetries are satisfied, appropriate topological

invariants can be obtained from the bulk properties of the material [8, 9]. The *bulk-edge correspondence* then allows one to relate these invariants with the presence of edge or interface localized modes [10, 11]. Despite the broad applicability of the principle, a precise statement of the bulk-boundary correspondence depends on the symmetry class, the dimensionality and the type of topological invariant. For this reason, providing a proof of this correspondence requires case-by-case analyses, with the most extensively studied case being 2D systems in the unitary class characterized by a Chern number [12, 13, 9].

In 1D continuous systems with mirror symmetry, the most popular invariant is the Zak phase [14], which can only take values 0 or π and remains constant until a Dirac point is reached. In this context, the Zak phases of contacting crystals govern the existence of localized modes. These modes are topologically protected in the sense that they are maintained by symmetry preserving continuous deformations of the medium, unless the gap is closed (Dirac point). In this context, two classes of methods have been used to analyze the existence of topological states and prove the bulk-edge correspondence. A first method consists of perturbing the Hamiltonian of the system studied, in the vicinity of a Dirac point [15, 16]. It therefore requires an *a priori* knowledge of Dirac points or their artificial construction by band-folding. A second approach consists in focusing on specific models, where the correspondence can be established by direct calculations [17]. Moreover, several works have exploited the concept of impedance [16, 17, 18, 19], which allows one to relate the existence of interface modes to bulk properties. This approach is elegant and offers a new point of view. However, it has been so far limited to specific examples or perturbative approaches. The objective of the present paper is to generalize the impedance approach to any PCs. This leads us to a proof the a stronger version of the bulk-edge correspondence for 1D continuous systems with mirror symmetry. We also point out that several authors have analyzed the somewhat related but different problem of localized modes for 1D PCs with parameter dependent interfaces, and their relations to Chern numbers [20, 21].

For this purpose, the sketch of the study is as follows. Section 2 describes elastic PCs, where classical band structure results are recalled. Section 3 focuses on the particular case of mirror symmetric PCs. The symmetry properties of Bloch modes at band edges are proven, based on some existing results. Section 4 investigates two semi-infinite PCs in contact. The concept of surface impedance is introduced. When the frequency varies in a gap, a strict decay of the surface impedance is proven (Lemma 4). This key result allows to prove Theorem 1, which recovers the existing results on topologically protected interface modes. The absence of such modes with Neumann or Dirichlet conditions is also explained, contrary to the discrete case such as SSH (Su-Schrieffer-Heeger). The latter is the simplest 1D model ensuring a nontrivial topology [22, 8, 23]. Section 5 proposes a generalized framework to extend the Theorem 1, notably allowing to treat the case of subwavelength PCs with Helmholtz resonators or dispersive media. Lastly, Section 6 concludes the paper and proposes some future directions of

investigations.

2. Problem statement

This section starts with a presentation of the physical problem addressed. After that and for completeness, we collect several known results about the spectrum of a periodic differential operator. The readers are referred to [4, 26, 27] for more details about the Bloch-Floquet theory.

2.1. Physical modeling

We consider linear elastic wave propagation at a given angular frequency $\omega = 2\pi f$. The medium is h-periodic with mass density $\rho(x)$ and Young's modulus $E(x)$ which are purely real, so that dissipation is neglected. The displacement $u(x)$ satisfies the Helmholtz equation

$$\frac{d}{dx}\left(E(x)\,\frac{du}{dx}\right) + \rho(x)\,\omega^2\,u = 0. \tag{1}$$

The equation (1) is generic for different wave physics. For instance, the case of acoustics is obtained changing u by the acoustic pressure p, E by $1/\rho$, and ρ by $1/\kappa$, where $\kappa = \rho c^2$ is the modulus of compressibility. Similarly, the case of photonics is obtained by changing ρ by the permittivity ϵ and E by $1/\mu$, where μ is the permeability. Without loss of generality, the edges of the periodic cells are assumed to be located at nh, with $n \in \mathbb{Z}$. The physical parameters are piecewise smooth, L^∞ and strictly positive.

2.2. Band structure

We denote $L^2[0,h]$ the Hilbert space equipped with the weighted inner product

$$\langle v|w\rangle = \int_0^h \rho(x)\,v(x)\,\overline{w}(x)\,dx, \tag{2}$$

where $\overline{w}$ refers to the complex conjugate of w. Let $\mathcal{B} = [-\pi,\pi]$ be the first Brillouin zone. The Bloch Hamiltonian $\mathcal{L}(q)$ is defined as the linear operator

$$\mathcal{L}(q)u = -\frac{1}{\rho(x)}\,\frac{d}{dx}\left(E(x)\,\frac{du}{dx}\right) \text{ for } x \in \mathbb{R}, \tag{3}$$

together with the Bloch-Floquet condition $u(h) = e^{\mathrm{i}q}\,u(0)$. Given a Bloch wavenumber $q \in \mathcal{B}$, the Bloch Hamiltonian yields a q-dependent eigenvalue problem on $\mathbb{R}$: find (λ, u) such that

$$\begin{cases} \mathcal{L}(q)u = \lambda u, \\ \quad u(h) = e^{\mathrm{i}q}\,u(0), \end{cases} \tag{4}$$

in the function space

$$L^2_q = \{g \in L^2[0,h] \,:\, g(h) = e^{\mathrm{i}q}\,g(0)\}.$$

The eigenvalue λ is the square angular frequency that appears in the Helmholtz equation (1): $\lambda = \omega^2$. The eigenvalue problem (4) has a an infinite set of (possibly repeated) real positive eigenvalues $\lambda_n(q) := \omega_n^2(q)$ ordered by increasing value:

$$\lambda_1(q) \leq \lambda_2(q) \leq \cdots \leq \lambda_n(q) \leq \cdots$$

The dispersion relations of the nth band $q \to \lambda_n(q)$ are continuous with respect to $q \in \mathcal{B}$ and monotonically increasing or decreasing on each half of the Brillouin zone, i.e. $[-\pi, 0]$ and $[0, \pi]$ [4, 28]. Moreover, they satisfy $\lambda_n(-q) = \lambda_n(q)$, as imposed by reciprocity. The eigenfunctions u_n are called Bloch modes, and they are orthogonal for the inner product (2). Lastly, $\lambda_1(0) = 0$, and the corresponding Bloch mode is a constant function. For each integer n, let

$$\lambda_n^- = \min\{\lambda_n(q) : q \in \mathcal{B}\}, \qquad \lambda_n^+ = \max\{\lambda_n(q) : q \in \mathcal{B}\}.$$

Then the entire spectrum of the Hamiltonian is given by

$$\sigma(\mathcal{L}) = \bigcup_{n \geq 1} [\lambda_n^-, \lambda_n^+],$$

which corresponds to the essential part of the spectrum. The interval $[\lambda_n^+, \lambda_{n+1}^-]$ is a gap if $\lambda_n^+ < \lambda_{n+1}^-$ for some n.

3. Phononic crystals with mirror symmetry

3.1. Parity of Bloch modes

From now on, we consider a particular case of periodic media, which are mirror symmetric, or equivalently reflection symmetric with respect to the centre of each cell. On $[0, h]$, we thus have $\rho(x) = \rho(h - x)$ and $E(x) = E(h - x)$. One introduces the parity operator $\mathcal{P}$, such that $(\mathcal{P}f)(x) = f(h - x)$. Mirror symmetry implies that

$$\mathcal{P}\,\mathcal{L}(-q) = \mathcal{L}(+q)\,\mathcal{P}, \qquad \forall q \in \mathcal{B}. \tag{5}$$

Since $\mathcal{L}(-\pi) = \mathcal{L}(\pi)$, it follows from (5) that the Hamiltonian and the parity operator commute at the band edges $q = 0$ and $q = \pm\pi$.

Let us consider an eigenvector $u_n(q)$ of $\mathcal{L}(q)$, with eigenvalue $\lambda_n(q)$. Then (5) gives that $\mathcal{P}u_n(q)$ is an eigenvector of $\mathcal{L}(-q)$ with the same eigenvalue $\lambda_n(q)$. Moreover, $u_n(-q)$ is also an eigenvector of $\mathcal{L}(-q)$ with eigenvalue $\lambda_n(q)$. Assuming that $\lambda_n(q)$ is a non-degenerate eigenvalue (non-overlapping bands), it means that $u_n(-q)$ and $\mathcal{P}u_n(q)$ are proportional to one another. Since $\mathcal{P}$ is unitary, it follows

$$u_n(-q) = \mu\,\mathcal{P}u_n(q) = e^{\mathrm{i}\,\xi_n(q)}\mathcal{P}u_n(q), \tag{6}$$

where $\xi_n(q)$ is a real and locally smooth function of q. At the band edges ($q = 0, \pi$), applying $\mathcal{P}$ on both sides of (6) and using the symmetry $\mathcal{P}^2 = 1$ gives $\mu^2 = 1$. As a consequence $\mu = \{\pm 1\}$

and $\xi_n = \{0, \pi\}$ at the band edges. The case $\mu = +1$ (and $\xi_n = 0$) gives $u_n(q) = \mathcal{P}u_n(q)$: the Bloch mode is symmetric, and u_n' is anti-symmetric, where prime denotes the space derivative. Conversely, in the case $\mu = -1$ (and $\xi_n = \pi$), then $u_n(q) = -\mathcal{P}u_n(q)$: the Bloch mode is anti-symmetric, and u_n' is symmetric. We introduce the spaces of symmetric functions $\mathcal{S}$ and anti-symmetric functions $\mathcal{A}$

$$\mathcal{S} = \{g : \mathcal{P}g = +g\}, \qquad \mathcal{A} = \{g : \mathcal{P}g = -g\}. \tag{7}$$

Then the properties of Bloch modes at the edges of the gaps (or simply "band edges") are summed up as follows.

Lemma 1. *Let us consider a mirror symmetric PC. We assume that the nth eigenvalues of the Hamiltonian are not degenerate at $q = 0$ and π. Then the following alternative holds at the band edges:*

- *either $u_n \in \mathcal{S}$ and $u_n' \in \mathcal{A}$;*
- *or $u_n \in \mathcal{A}$ and $u_n' \in \mathcal{S}$.*

The values of $u_n(0)$ and $u_n'(0)$ are deduced from the Lemma 1. First of all, $u_n(0)$ and $u_n'(0)$ cannot be simultaneously zero (and similarly at h). By uniqueness of the solution of (1), this would imply that u_n is identically null.

	$q = 0$	$q = \pi$
$u_n \in \mathcal{S}$	$u_n'(0) = 0$	$u_n(0) = 0$
$u_n \in \mathcal{A}$	$u_n(0) = 0$	$u_n'(0) = 0$

Table 1: Values of the Bloch modes $u_n(0)$ and $u_n'(0)$ at the edges of the nth gap. The cases are distinguished according to the symmetry of u_n and the value of q.

Then, let us first consider $q = 0$ and assume that $u_n \in \mathcal{S}$. The Lemma 1 implies $u_n' \in \mathcal{A}$, and hence $u_n'(h) = -u_n'(0)$. But the Bloch-Floquet condition gives $u_n'(h) = e^{\mathrm{i}0}u_n'(0) = +u_n'(0)$, and thus $u_n'(0) = -u_n'(0) = 0$. If $u_n \in \mathcal{A}$, then similar arguments yield $u_n(0) = -u_n(0) = 0$. At $q = \pi$, the Bloch-Floquet conditions gives $u_n(h) = e^{\mathrm{i}\pi}u_n(0) = -u_n(0)$ and $u_n'(h) = -u_n'(0)$. If $u_n \in \mathcal{S}$ then $u_n(0) = 0$. Conversely, if $u_n \in \mathcal{A}$ then $u_n' \in \mathcal{S}$ and $u'(0) = 0$. All these cases are summarized in the Table 1.

Figure 1 illustrates these different cases. The physical and geometrical parameters correspond to the configuration studied in Section 5.4 (with the interface spacing $\theta = 0.25$), and will be described later. For the moment, it is sufficient to observe the symmetry properties. Figure 1 represents the Bloch mode at $q = \pi$ and at frequencies of the band edges of the first gap. At

the entry frequency λ_1^+ of gap 1 (a), u_1 is symmetric. As written in Table 1, u_1 is therefore symmetric and cancels at $x = 0$ and $x = h$. On the contrary, u_2 is antisymmetric at the exit frequency λ_2^- of the gap 1 (b), leading to $u_2'(0) = u_2'(h) = 0$.

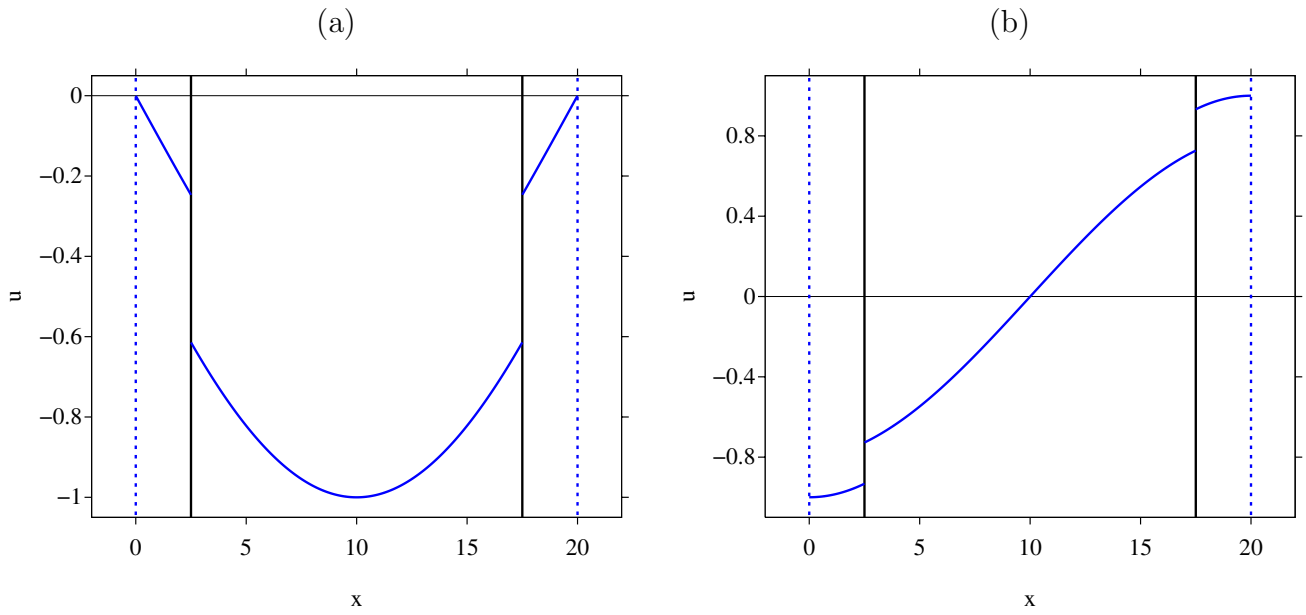

Figure 1: Bloch mode at the edges of gap 1 ($q = \pi$). (a): entry of the gap λ_1^+; (b): exit of the gap λ_2^-. The vertical solid lines denote the imperfect interfaces. The vertical dotted lines denote the edges of the elementary cell. The physical parameters are described in Section 5.4.

3.2. Change of parity across a gap

Here we investigate the change of parity of the Bloch modes at $q = 0$ or $q = \pi$ when the frequency crosses a gap. The proof relies on the oscillation theory of Sturm-Liouville operators, see for instance [29, 27, 16]. Let us denote λ_j^P, λ_j^A, λ_j^D, and λ_j^N the jth eigenvalues of the Hamiltonian $\mathcal{H}$ on the elementary cell $[0, h]$, respectively associated with the following boundary conditions:

1. periodic boundary conditions: $u(h) = u(0)$, $u'(h) = u'(0)$, which is the Bloch condition at $q = 0$;
2. antiperiodic boundary conditions: $u(h) = -u(0)$, $u'(h) = -u'(0)$, which is the Bloch condition at $q = \pi$;
3. Dirichlet boundary conditions: $u(h) = u(0) = 0$;
4. Neumann boundary conditions: $u'(h) = u'(0) = 0$.

As stated in Theorem 13-10 of [29], these eigenvalues satisfy the interlacing property:

$$\begin{aligned}&\lambda_1^N \leq \lambda_1^P < \lambda_1^A \leq \{\lambda_2^N, \lambda_1^D\} \leq \lambda_2^A < \lambda_2^P \leq \{\lambda_3^N, \lambda_2^D\} \leq \cdots \\ &\cdots \leq \lambda_{2n-1}^P < \lambda_{2n-1}^A \leq \{\lambda_{2n}^N, \lambda_{2n-1}^D\} \leq \lambda_{2n}^A < \lambda_{2n}^P \leq \{\lambda_{2n+1}^N, \lambda_{2n}^D\} < \lambda_{2n+1}^P \leq \cdots\end{aligned} \tag{8}$$

In substance, this says that there is a single Neumann and a single Dirichlet eigenvalue inside each gap (possibly closed) of the corresponding periodic problem. This leads to the following result (see Theorem 4.4 of [16]):

Lemma 2. *Let us consider a mirror symmetric PC, where the jth band is isolated. Then the Bloch modes on each edge of a gap, i.e. (q, λ_j^+) and (q, λ_{j+1}^-) with $q = 0$ or $q = \pi$, attain different symmetries.*

In other words, if $u_n \in \mathcal{S}$ then $u_{n+1} \in \mathcal{A}$, and inversely. To show this, we first notice that the boundary values in Table 1 imply that the Bloch mode on each edge of the nth gap satisfy either Neumann or Dirichlet boundary conditions. Using the interlacing property (8), we conclude that there is a single Neumann and a single Dirichlet eigenvalue on the gap edges. Lemma 2 then follows.

3.3. Relation between Zak phase and Bloch mode symmetry

Bands of a mirror symmetric 1D PC possess topological properties characterized by an invariant called the Zak phase. To define it, we introduce the Berry connection $A_n(q)$ of the nth band:

$$A_n(q) = -\mathrm{i}\,\langle u_n(q) | \partial_q u_n(q) \rangle\,, \tag{9}$$

where $\langle . | . \rangle$ is the Hermitian inner product (2). The integral of the Berry connection across the first Brillouin zone gives the Zak phase:

$$\Phi_n = \int_{-\pi}^{+\pi} A_n(q)\, dq. \tag{10}$$

Notice that the Zak phase is defined using the Bloch mode $u_n(q)$, which is not periodic in x, but periodic in q (see equation (4)). In the case of a periodic and mirror symmetric medium, and assuming that the nth eigenvalue is non-degenerate (no Dirac point), the Zak phase is directly given by the change of symmetry from one edge of the band to the other, namely:

$$\Phi_n = \xi_n(\pi) - \xi_n(0), \tag{11}$$

where ξ is defined in (6). A proof of (11) is given in Appendix A. The Zak phase is defined mod 2π, and it can be either 0 (trivial) or π (topological).

As we shall see in Section 4, the existence of an interface localized mode depends on the symmetries on each edge of a given gap, i.e. at λ_n^+ and λ_{n+1}^-. As we already saw (see Lemma

2), the two symmetries are necessarily different, so it is sufficient to know the mode symmetry at λ_n^+. Hence, we define the bulk topological index of the gap n as $\mathcal{J}_n$:

$$\mathcal{J}_n = \begin{cases} +1 & \text{if } u_n^+ \in \mathcal{S}, \\ -1 & \text{if } u_n^+ \in \mathcal{A}. \end{cases} \tag{12}$$

Now, since the Bloch mode at zero frequency ($\lambda_1(0) = 0$) is always symmetric ($u_1^- \in \mathcal{S}$), we can obtain the symmetry at the entry of a given gap by checking how many symmetry changes occur when the frequency ranges from 0 to λ_n^+: for each gap there is a change, and for each band there is a change if it is topological and none if it is trivial. As shown in [17, 16], this translates into

$$\mathcal{J}_n = (-1)^{n-1} \prod_{j=1}^{n} e^{\mathrm{i}\,\Phi_j}. \tag{13}$$

4. Semi-infinite phononic crystals

4.1. Surface impedance

From now on, we consider two semi-infinite PCs in contact at $x = 0$. The interface at $x = 0$ is at the boundary of the unit cells for both the left and right PC, and u and $E\,u'$ are continuous across the interface. The features of the PCs on the left ($x < 0$) and right ($x > 0$) are denoted by the indices L and R, respectively. For instance, the Hamiltonians are $\mathcal{L}_L$ and $\mathcal{L}_R$, with eigenvalues $\lambda_{n,L}$ and $\lambda_{n,R}$. In each PC, the parameters are spatially periodic and with mirror symmetry. For simplicity, we assume that the periods are identical and equal to h, without this being restrictive.

Let us assume that the intersection of the nth gaps of the two Hamiltonians is non empty:

$$\Omega_n = [\lambda_{n,L}^+, \lambda_{n+1,L}^-] \cap [\lambda_{n,R}^+, \lambda_{n+1,R}^-] := [\lambda_n^+, \lambda_{n+1}^-] \neq \emptyset. \tag{14}$$

For simplicity, we assumed the left and right gaps to be labeled by the same number n, but our results stand for any two gaps n_L and n_R as long as the intersection Ω as in equation (14) is non-empty. For further use, $u_{n,L}^+$ denotes the Bloch mode for the eigenvalue $\lambda_{n,L}^+$; similarly $u_{n,R}^+$ denotes the Bloch mode for the eigenvalue $\lambda_{n,R}^+$.

The wave fields with frequency in this gap, solution of equation (1), can be decomposed into two modes, one increasing exponentially and the other decreasing exponentially as $|x| \to +\infty$. For frequencies inside Ω_n, one defines *surface impedances* of PC-L and PC-R [17]:

$$Z_L(\omega) = -\frac{u(0^-, \omega)}{E(0^-)\,u'(0^-, \omega)}, \qquad Z_R(\omega) = +\frac{u(0^+, \omega)}{E(0^+)\,u'(0^+, \omega)}, \tag{15}$$

where u is the unique solution decreasing when $x \to -\infty$ for Z_L and when $x \to +\infty$ for Z_R. Inside a gap, u and u' are real, and hence $Z_{L,R}$ are real. Hereafter, we will simply write Z to characterise the generic properties of the surface impedance, independently of the medium

considered. We will refer to both λ and ω, with $\lambda = \omega^2$, as the frequency, depending on the context. Lastly, the notation Z_n will denote the surface impedance at λ_n.

The notion of surface impedance will be fundamental in the rest of the paper. An interface mode at $x = 0$ corresponds to two evanescent modes satisfying the continuity conditions $u(0^-, \omega) = u(0^+, \omega)$ and $E(0^-)\, u'(0^-, \omega) = E(0^+)\, u'(0^+, \omega)$. This leads to the following Lemma.

Lemma 3. *A necessary and sufficient condition for the existence of an interface localized mode in Ω_n is*

$$Z_L(\omega) + Z_R(\omega) = 0, \qquad \omega \in \Omega_n. \tag{16}$$

To determine the existence of a solution to (16), we study the properties of Z in the gaps. The first key element is that the impedance value at the edges of a gap is given by the symmetries of Bloch modes. Indeed, at the edges of a gap, $u := u_n$ and $u' := u_n'$. Based on the definition of Z and on Table 1, the surface impedance Z_n on the edges of a gap is either 0 or ∞, depending on the symmetry of u_n. This is summarized in Table 2.

	$q = 0$	$q = \pi$
$u_n \in \mathcal{S}$	$Z_n = \pm\infty$	$Z_n = 0$
$u_n \in \mathcal{A}$	$Z_n = 0$	$Z_n = \pm\infty$

Table 2: Surface impedance Z_n on the edges of the Brillouin zone and at the edges of the nth gap, depending on the symmetry of the Bloch mode u_n.

At this level, it is tempting to use a continuity argument to find solutions of equation (16), i.e. interface modes. Table 2 is however not enough to conclude, since we don't control the sign of the impedance. To do so, we will now investigate the evolution with the frequency of Z_L and Z_R inside a gap.

4.2. Monotony of the surface impedances in gaps

We now discuss a key new result, which will allow us to make strong statement regarding the bulk-boundary correspondence: the in-gap impedance obtained from equation (1) is always a decreasing function of the frequency. For this purpose, one differentiates the Helmholtz equation (1) with respect to ω. Setting $\varphi = \frac{du}{d\omega}$, one obtains

$$\frac{d}{dx}\left(E(x)\frac{d\varphi}{dx}\right) + \rho(x)\,\omega^2\,\varphi = -2\,\rho(x)\,\omega\,u. \tag{17}$$

From the definition of Z_R in (15), it follows

$$\frac{dZ_R}{d\omega} = \frac{\mathcal{W}(0^+, \omega)}{\left(E(0^+)\,u'(0^+)\right)^2}, \tag{18}$$

with the Wronskian

$$\mathcal{W}(x,\omega) = E(x)\left(\varphi(x)\,u'(x) - u(x)\,\varphi'(x)\right). \tag{19}$$

The prime means the derivative with respect to x. The Wronskian is then differentiated with respect to x. Using (1) and (17) gives

$$\begin{aligned} \mathcal{W}' &= \varphi\,(E\,u')' - u\,(E\,\varphi')', \\ &= \varphi\,\left(-\rho\,\omega^2\,u\right) - u\,\left(-2\,\rho\,\omega\,u - \rho\,\omega^2\,\varphi\right), \\ &= 2\,\rho\,\omega\,u^2. \end{aligned} \tag{20}$$

The latter is integrated with respect to x on PC-R:

$$\mathcal{W}(+\infty,\omega) - \mathcal{W}(0,\omega) = 2\,\omega\int_0^{+\infty}\rho\,u^2\,dx. \tag{21}$$

In the gap, the evanescent field vanishes when $x \to +\infty$, and hence $\mathcal{W}(+\infty,\omega) = 0$. Using (18) and the fact that u is real in a gap leads to

$$\frac{dZ_R}{d\omega} = -\frac{2\,\omega}{\left(Eu'(0^+)\right)^2}\int_0^{+\infty}\rho\,u^2\,dx < 0. \tag{22}$$

A similar argument is used to prove that the left surface impedance decreases: $\frac{dZ_L}{d\omega} < 0$ in a gap. These results are summed up in the next Lemma.

Lemma 4. *In a given gap* $]\lambda_n^+, \lambda_{n+1}^-[$*, the surface impedance decreases with frequency:*

$$\frac{dZ}{d\omega} < 0, \qquad \omega \in]\lambda_n^+, \lambda_{n+1}^-[. \tag{23}$$

Lemma 4 implies that Z never vanishes and never becomes infinite inside a gap. Indeed, let us assume for instance that $u_n \in \mathcal{S}$ at $q = 0$. Table 2 states that $Z := Z_n = \pm\infty$ at λ_n^+. In the gap Ω_n, Z decreases monotonically, and Lemma 2 states that $u_{n+1} \in \mathcal{A}$, so that $Z = 0$ at λ_{n+1}^-. It fixes the sign $Z_n = +\infty$ at λ_n^+ and ensures that $Z \neq 0$ and $Z \neq \infty$ on $]\lambda_n^+, \lambda_{n+1}^-[$. A similar argument can be used with $u_n \in \mathcal{A}$ at $q = 0$, and also at $q = \pi$. An alternative proof of this Lemma based on the transfer matrix is proposed in Appendix B.

4.3. Topologically protected interface mode

Now we are ready to state the main result of this article.

Theorem 1. *Let two mirror symmetric PCs in perfect contact at* $x = 0$ *with a non-empty common gap* Ω_n (14)*. Let also* $\mathcal{J}_{n,L}$ *and* $\mathcal{J}_{n,R}$ *be the bulk topological indices* (12) *of PC-L and PC-R, respectively. Without change of symmetry in left and right Bloch modes, ie*

$$\mathcal{J}_{n,L} + \mathcal{J}_{n,R} \neq 0, \tag{24}$$

then no interface mode exists. In the opposite case of left and right Bloch modes with different symmetries, ie

$$\mathcal{J}_{n,L} + \mathcal{J}_{n,R} = 0, \tag{25}$$

then there exists a unique interface mode in Ω_n at $\lambda_n^\sharp$. This mode is topologically protected as it is maintained by continuous transformations of the PCs as long as no Dirac point is reached.

Proof. Let us assume that the mode symmetries are the same for each PC and two overlapping gaps (trivial interface). For instance, $u_{n,L}^+ \in \mathcal{S}$ and $u_{n,R}^+ \in \mathcal{S}$ at $q = 0$. Table 2 and Lemma 4 imply that Z_L decreases from $+\infty$ to 0 when the frequency varies from $\lambda_{n,L}^+$ to $\lambda_{n+1,L}^-$. Similarly, Z_R decreases from $+\infty$ to 0 when the frequency varies from $\lambda_{n,R}^+$ to $\lambda_{n+1,R}^-$. It follows that $Z_L + Z_R > 0$ never vanishes on Ω_n. Lemma 3 ensures thus that no interface mode exists. The proof in the cases $u_{n,L}^+ \in \mathcal{A}$ and $u_{n,R}^+ \in \mathcal{A}$, as well as $q = \pi$, follows exactly the same lines.

Next one considers the case of opposite symmetries, say $u_{n,L}^+ \in \mathcal{S}$ and $u_{n,R}^+ \in \mathcal{A}$ at $q = 0$, (topological interface). As in the previous case, Z_L decreases from $+\infty$ to 0 when the frequency varies from $\lambda_{n,L}^+$ to $\lambda_{n+1,L}^-$. But the antisymmetry of $u_{n,R}^+$ implies that Z_R decreases from 0 to $-\infty$ when the frequency varies from $\lambda_{n,R}^+$ to $\lambda_{n+1,R}^-$. Now, the lower edge of the gap is at $\lambda_{n,L}^+$ or at $\lambda_{n,R}^+$. At that lower edge, $Z_L + Z_R$ is always strictly positive: in the first case, $(Z_L + Z_R)_{\lambda=\lambda_{n,L}^+} = +\infty$, while in the second case $(Z_L + Z_R)_{\lambda=\lambda_{n,R}^+} = Z_L(\lambda_{n,R}^+) > 0$. Similarly, on the upper edge, either at $\lambda_{n+1,L}^-$ or at $\lambda_{n+1,R}^-$, $Z_L + Z_R$ is always strictly negative: $(Z_L+Z_R)_{\lambda=\lambda_{n+1,L}^-} = Z_R(\lambda_{n+1,L}^-) < 0$ in the first case and $(Z_L+Z_R)_{\lambda=\lambda_{n+1,L}^-} = -\infty$ in the second case. Hence, by continuity and monotony of $Z_L + Z_R$ (Lemma 4), it vanishes a single time in the Ω_n interval. From Lemma 3, there is a unique interface localized mode in this frequency interval.

As indicated in Section 3.3, the symmetries of $u_{n,L}^+$ and $u_{n,R}^+$ are maintained by continuous deformations of the nth band, as long as it remains isolated. Since the interface mode is a direct consequence of the symmetries of Bloch modes, it is topologically protected. □

4.4. Absence of edge mode for one-sided systems

In the particular case of a single PC with Dirichlet boundary condition ($u(0,\omega) = 0$) or Neumann boundary condition ($E\,u'(0,\omega) = 0$), then only one surface impedance is involved, for instance Z_R. A mode localized near $x = 0$ will exist if and only if $Z_R = 0$ for a Neumann boundary condition and $Z_R = \infty$ for a Dirichlet one. In this case, we talk about edge modes rather than interface modes. However, at the entry of the nth gap Ω_n, it takes the value $Z_n = 0$ or $Z_n = +\infty$, respectively. Z then decreases monotonically and never vanishes nor becomes infinite. This was already mentioned after Lemma 4, but it results in the following Theorem.

Theorem 2. *Let us consider one semi-infinite mirror symmetric PC, with Dirichlet or Neumann boundary conditions. Then no edge mode exists.*

This is a rather surprising result. First, it is in direct contrast with discrete systems (e.g. lattice models) where edge modes can be found and protected by a quantized Zak phase. Second, it shows explicitly that the bulk-boundary correspondence only works for interfaces in the case of continuous systems with mirror symmetry. A third striking consequence of Theorem 2 is that edge modes (with Dirichlet or Neumann boundary conditions) may exist only if one breaks the mirror symmetry (either in the bulk or by an appropriate choice of edge). This is the case for instance in the waveguide realisation of SSH [23].

Moreover, our results allow us to treat the case of (non-dissipative) Robin boundary conditions quite easily. To see this, we define such a boundary condition in the form of an impedance condition, consistent with equation (15):

$$E(0)u'(0,\omega) = -Z_0 u(0,\omega),$$

where $Z_0 \in \mathrm{i}\mathbb{R}$. Similarly to Lemma 3, an edge mode exists in a given gap under the condition that:

$$Z_0 + Z_R(\omega) = 0.$$

From this and Lemma 4 we directly conclude that there is a unique edge mode if $\Im(Z_0)$ has the opposite sign with respect to $\Im(Z_R(\omega))$, and no edge mode if they have the same sign.

Another natural one-sided system is that formed by the interface between a semi-infinite PC and a homogeneous material. In this case however, since no evanescent mode exists in the homogeneous media there can be no interface localized mode.

4.5. Numerical example: the bilayer model

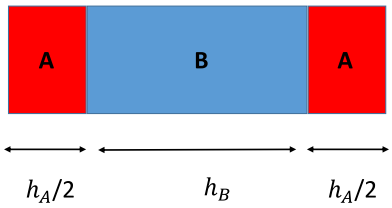

Figure 2: Elementary cell with phases A and B.

Let us consider a bilayered periodic structure AB, each phase having length h_i, density ρ_i and wave velocity $c_i = \sqrt{E_i/\rho_i}$, with $i = A, B$ (Figure 2). The total length of an elementary cell is $h = h_A + h_B$. The phases are in perfect contact. The ratio of propagation times in each phase is assumed to be commensurable:

$$\alpha = \frac{\dfrac{h_A}{c_A}}{\dfrac{h_B}{c_B}} = \frac{h_A\, c_B}{h_B\, c_A} := \frac{m_1}{m_2} \in \mathbb{Q}.$$

There is then a Dirac point separating the spectral bands m_1+m_2 and m_1+m_2+1 (numbering by 1 the first band starting at $(q=0,\omega=0)$). As proven in Appendix A of [17], this Dirac point is located at frequency

$$f=\frac{m_1+m_2}{2\,\tau},\qquad \text{with } \tau=\frac{h_A}{c_A}+\frac{h_B}{c_B}.$$

Here we follow the configuration used in [17, 37]: taking

$$\begin{cases}(h_A=4,\rho_A=1000,c_A=4000) & \text{(phase A)}\\ (h_B=6,\rho_B=1000,c_B=4000) & \text{(phase B)}\end{cases}$$

yields $m_1=4$ and $m_2=3$: bands 7 and 8 intersect at a Dirac point at the scaled frequency $\tilde{f}=f\times h/c=2.5$, where $c=c_B=4000$ is a normalization frequency (Figure 3-(a)).

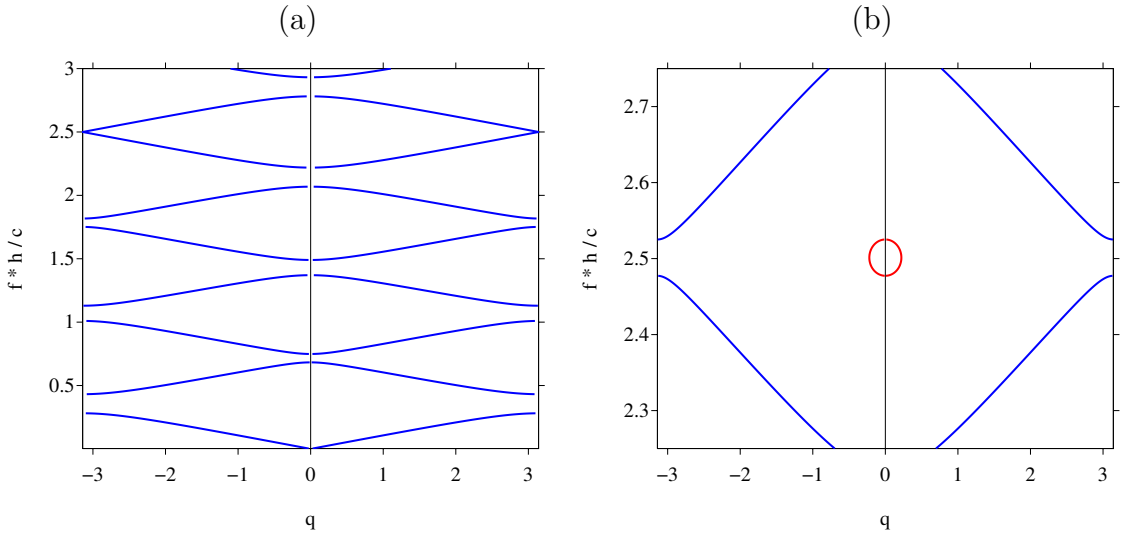

Figure 3: (a) Bloch-Floquet dispersion diagrams, for various values of ν. (a): $\nu=2$, where bands 7 and 8 cross at a Dirac point at scaled frequency 2.5. (b): $\nu=1.95$, with a zoom on the gap between bands 7 and 8. The red curves are the imaginary values of q.

This configuration is modified through a parameter ν: the celerity in phase A becomes $c_{A'}=c_A/\nu$, the other physical parameters being unchanged. To maintain similar midgap positions, the shift τ must remain constant. It implies to modify the lengths through the relations

$$h_{A'}=h_A\frac{\dfrac{1}{c_A}-\dfrac{1}{c_B}}{\dfrac{1}{c_{A'}}-\dfrac{1}{c_B}},\quad h_{B'}=h-h_{A'}. \tag{26}$$

Taking $\nu=1.95$ opens a gap Ω_7 around $\tilde{f}=2.5$ (Figure 3-(b)), with a symmetrical Bloch mode at $\tilde{f}_7$. On the contrary, the gap opened using $\nu=2.05$ yields an asymmetrical Bloch mode at $\tilde{f}_7$.

		$n=6$	$n=7$	$n=8$
PC-L	$[\tilde{f}_n^+, \tilde{f}_{n+1}^-]$	[2.068, 2.216]	[2.477, 2.525]	[2.794, 2.916]
	symmetries	$\mathcal{S}$	$\mathcal{S}$	$\mathcal{A}$
PC-R	$[\tilde{f}_n^+, \tilde{f}_{n+1}^-]$	[2.073, 2.214]	[2.475, 2.522]	[2.777, 2.936]
	symmetries	$\mathcal{S}$	$\mathcal{A}$	$\mathcal{A}$

Table 3: Scaled frequency intervals of the gaps $n = 6$, 7, 8. Symmetries of the Bloch modes at scaled frequencies $\tilde{f}_n^+$, in PC-L ($\nu = 1.95$) and PC-R ($\nu = 2.05$).

Two semi-infinite PCs are then built using $\nu = 1.95$ ($x < 0$) and $\nu = 2.05$ ($x > 0$). They are denoted by PC-L and PC-R, respectively. The scaled frequencies and the symmetry of u_n at the band edges of their respective gaps $n = 6$, 7, 8 are given in Table 3. We observe that the band edges of PC-L and PC-R are close but different; the construction method detailed above only ensures equality of the midgaps. Their intersections are denoted by Ω_n. Moreover, the symmetries of the Bloch modes are unchanged in the cases $n = 6$ and $n = 8$. On the contrary, the opening of the Ω_7 gap obtained by varying ν leads to a symmetry inversion. Based on Theorem 1, we expect the existence of a topologically protected interface mode in the gap Ω_7.

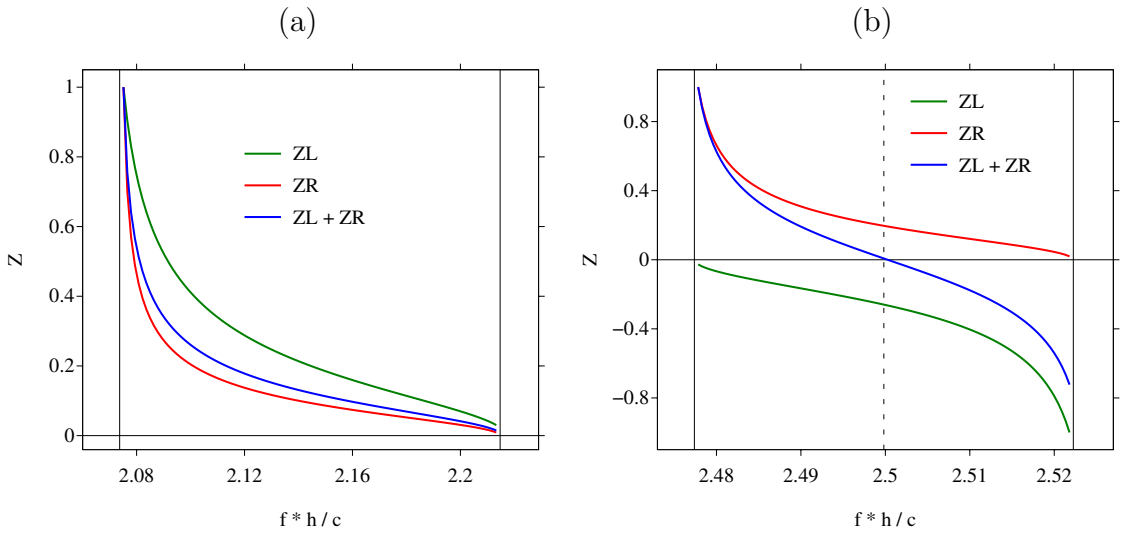

Figure 4: Frequency evolution of the surface impedances of the PCs in contact. The vertical solid lines denote the edges of the gap in scaled frequency. (a): gap Ω_6, in which no topologically protected interface mode exists. (b): gap Ω_7, in which a topologically protected interface mode exists. The vertical dotted line denotes the scaled frequency $\tilde{f}_7^\sharp \approx 2.50$ where $Z_L + Z_R = 0$.

Figure 4 shows the frequency evolution of the surface impedance Z_L in PC-L, of the surface impedance Z_R in PC-R, and finally of their sum, in the gaps Ω_6 and Ω_7. In Figure 4-(a), we observe that $Z_L + Z_R \neq 0$ on Ω_6: no interface mode exists. In Figure 4-(b), we observe that $Z_L + Z_R = 0$ at $\tilde{f}_7^\sharp \approx 2.50$ in gap Ω_7: according to Lemma 3, a topologically protected interface mode exists at this frequency.

We look for the expected interface modes in a scattering configuration. For this purpose,

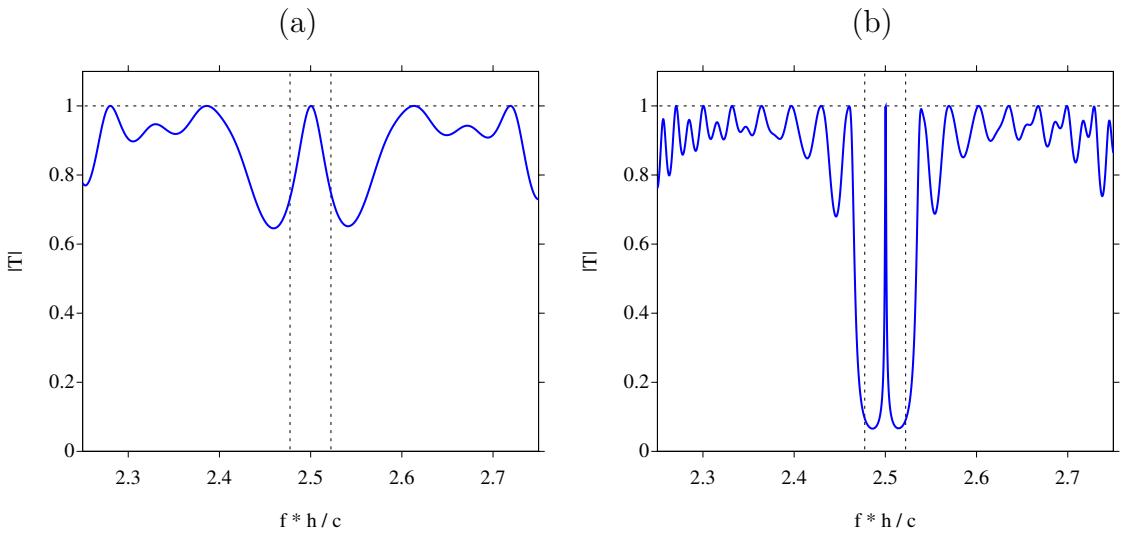

Figure 5: Modulus of the transmission coefficient in the case $N = 3$ cells (a) and $N = 10$ cells (b) per PC. The vertical dashed lines denote the lower and upper edges of Ω_7.

one considers finite PCs consisting of N PC-L on the left ($x < 0$), and N PC-R on the right ($x > 0$). Figure 5 shows the frequency evolution of the transmission coefficient on Ω_7 through the slab of $2N$ cells, for $N = 3$ (a) and $N = 10$ (b). A peak is observed in the Ω_7 gap, which becomes finer and finer as N increases. For $N = 10$, this peak is located at $\tilde{f} \approx 2.5$, which corresponds to the theoretical value $\tilde{f}_7^\sharp$.

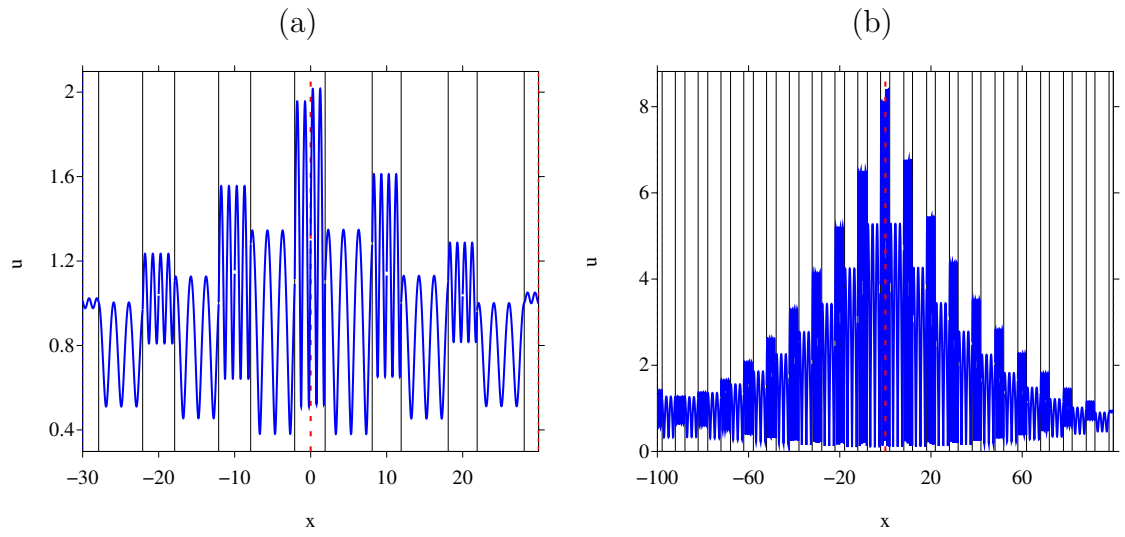

Figure 6: Spatial evolution of u at the scaled frequencies $\tilde{f}_7^\sharp = 2.5$. The vertical solid lines represent the interfaces. The red vertical dotted line at $x = 0$ denotes the interface between PC-L and PC-R, each being built with $N = 3$ cells (a) or $N = 10$ cells (b).

Figure 6 represents the spatial evolution of the modulus of u at $\tilde{f}_7^\sharp = 2.5$, with $N = 3$ cells (a) or $N = 10$ cells (b) in PC-L and PC-R. In both cases, an evanescent mode centered on the interface between the PCs is observed. It is a clear signature of an interface mode at the

interface between PC-L and PC-R.

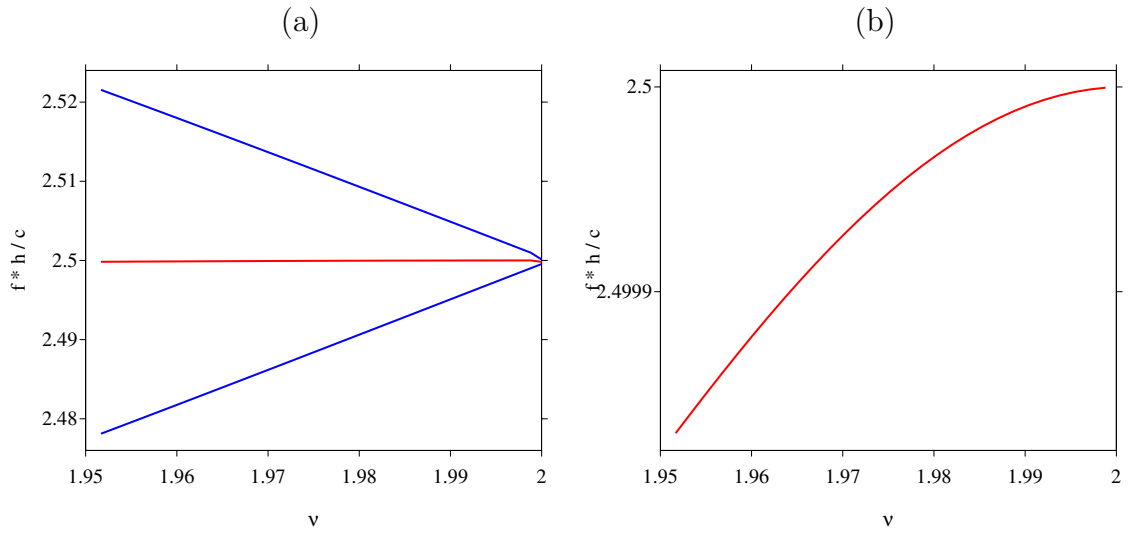

Figure 7: Frequency evolution of the topologically protected interface modes in the gap Ω_7, as a function of the parameter ν governing the properties of the elementary cell (26) (a). This scaled frequency $\tilde{f}_7^\sharp$ is represented by a red line. The blue curves represent the scaled lower edge $\tilde{f}_n^+$ and scaled upper upper $\tilde{f}_{n+1}^-$ of the gaps Ω_7. Zoom on $\tilde{f}_7^\sharp$ (b).

Finally, we study the evolution of the interface mode when the parameter ν varies in (26). Figure 7-(a) shows $\tilde{f}_7^\sharp$ as functions of ν. The blue lines denote the lower and upper edges of the gap Ω_7. The red line denotes the scaled frequency of the interface mode, computed as the zero of $Z_L + Z_R$. At the scale of the Figure, this frequency seems constant when ν varies, which shows the robustness of the topologically protected interface modes. Nevertheless, a large zoom on the red line shows that $\tilde{f}_7^\sharp$ is slighlty increasing with ν (b).

5. Generalizations

5.1. Framework

We now discuss some possible generalizations of the previous results. Our aim is to show that the bulk-boundary correspondence as established here, i.e. Theorem 1, stands for many popular cases beyond equation (1), for instance when resonators are added or with imperfect interfaces.

On the elementary cell $[0, h]$, a set of N interfaces is considered and is denoted by $\mathcal{I} = \{x_1, \cdots, x_N\}$. Between each interface, the Helmholtz equation takes the generalized form:

$$\frac{d}{dx}\left(A(x,\omega)\,\frac{du}{dx}\right) + V(x,\omega)\,u = 0, \tag{27}$$

where $A(x,.)$ and $V(x,.)$ are holomorphic real-valued function. In the case where $A(x,\omega) = E(x)$ and $V(x,\omega) = \rho(x)\omega^2$, we recover the Helmholtz equation (1).

At x_j, the fields satisfy the jump conditions:

$$[\![u]\!]_{x_j} = \alpha_j(\omega) \left\langle A \frac{du}{dx} \right\rangle_{x_j}, \qquad \left[\!\!\left[A \frac{du}{dx} \right]\!\!\right]_{x_j} = -\beta_j(\omega) \langle u \rangle_{x_j}, \tag{28}$$

with $\alpha_j(\omega) \geq 0$ and $\beta_j(\omega) \geq 0$ holomorphic. In (28), $[\![.]\!]_{x_j}$ and $\langle . \rangle_{x_j}$ denote the jump and the mean value at the interface x_j, respectively, and they are defined for any function $g(x)$ by

$$[\![g]\!]_{x_j} = g(x_j^+) - g(x_j^-), \qquad \langle g \rangle_{x_j} = \frac{1}{2} \left(g(x_j^+) + g(x_j^-) \right). \tag{29}$$

The PCs are still assumed to be mirror symmetric: A and V are even function of x for all ω, and the interfaces are placed symmetrically in each unit cells.

To prove the Theorem 1, we needed several spectral properties of the operator studied in Section 2. It means: i) a discrete spectrum at fixed Bloch wavenumber q; ii) a monotonic dispersion relation over half the Brillouin zone; iii) an inversion of symmetries at gap edges. In the following, we assume that property i) is always satisfied. Usually, it can be shown because the spectrum is that of a self-adjoint operator. Notice that in some cases, such as the Drude-Lorentz model (model 3 below), the spectrum can have an unusual structure, such as the presence of accumulation points [32]. Property ii) is always true for holomorphic frequency dispersions $A(x,\omega)$ and $V(x,\omega)$. Indeed, as stated in [28], this property comes from the second-order character of equation (1) at fixed frequency ω, and the uniqueness of the solution. This is unchanged in the generalization of equation (27), hence, this property is maintained. Lastly, the property iii) is proven in the Lemma 7 of Appendix B, using the transfer matrix method.

5.2. Bulk-boundary correspondence for a generalized Helmholtz equation

Here we want to generalize Theorems 1 and 2 to the general setting defined in the previous section. The key point is to prove that the decrease of $Z(\omega)$ across the gaps established in Section 4.2 still holds. The first difference is that now, the impedance defined in (15) has a frequency dependence through both the field and the coefficient $A(0^+,\omega)$. Hence, the equation (18) becomes

$$\frac{dZ_R}{d\omega} = \frac{1}{\left(A(0^+,\omega)\, u'(0^+)\right)^2} \left(\mathcal{W}(0^+,\omega) - \partial_\omega A(0^+,\omega)\, u(0^+)\, u'(0^+) \right), \tag{30}$$

with the Wronskian

$$\mathcal{W}(x,\omega) = A(x,\omega) \left(\varphi(x)\, u'(x) - u(x)\, \varphi'(x) \right). \tag{31}$$

Similarly to Section 4.2, to evaluate the sign of the Wronskian, we differentiate the generalized Helmholtz equation (27) with respect to ω yields outsides the interfaces:

$$(\partial_\omega A u')' + (A\varphi')' + \partial_\omega V\, u + V\, \varphi = 0. \tag{32}$$

Between each interface, the spatial evolution of the Wronskian (20) becomes

$$\mathcal{W}' = \partial_\omega V\, u^2 + u \left(\partial_\omega A\, u' \right)'. \tag{33}$$

To evaluate the Wronskian at the origin, it is integrated with respect to x on the PC-R. Using the decrease of evanescent fields at infinity, we get:

$$\mathcal{W}(0^+,\omega) = -\int_0^{+\infty} \mathcal{W}'(x)dx - \sum_{n=0}^{+\infty}\sum_{j=1}^{N} [\![W]\!]_{x_j+nh}\,. \tag{34}$$

The jumps of the Wronskian are evaluated in Lemma 8 proven in Appendix C. Using it, one obtains

$$\begin{aligned}\mathcal{W}(0,\omega) &= \partial_\omega A(0,\omega)\,u(0)\,u'(0) - \int_0^{+\infty} \partial_\omega V\ u^2\,dx + \int_0^{+\infty} \partial_\omega A\,u'^2\,dx \\ &- \sum_{n=0}^{+\infty}\sum_{j=1}^{N}\left(\partial_\omega\alpha_j\ \langle A\,u'\rangle^2_{x_j+nh} + \partial_\omega\beta_j\ \langle u\rangle^2_{x_j+nh}\right).\end{aligned} \tag{35}$$

Injecting the latter expression into (33), we obtain the frequency evolution of Z_R, which generalizes (22):

$$\begin{aligned}\frac{dZ_R}{d\omega} = &- \frac{1}{\left(A(0^+)u'(0^+)\right)^2}\left(\int_0^{+\infty} \partial_\omega V\,u^2\,dx - \int_0^{+\infty} \partial_\omega A\,u'^2\,dx\right. \\ &\left. + \sum_{n=0}^{+\infty}\sum_{j=1}^{N}\left(\partial_\omega\alpha_j\ \langle A\,u'\rangle^2_{x_j+nh} + \partial_\omega\beta_j\ \langle u\rangle^2_{x_j+nh}\right)\right).\end{aligned} \tag{36}$$

The sign of $\frac{dZ_R}{d\omega}$ depends obviously on the sign of $\partial_\omega A$, $\partial_\omega V$, $\partial_\omega\alpha_j$ and $\partial_\omega\beta_j$. A similar analysis can be performed on PC-L, yielding the following generalization of Lemma 4.

Theorem 3. *Let us consider mirror symmetric PCs described by equation (27) and the jump conditions (28). We assume that $A(x,.)$, $V(x,.)$, $\alpha_j(.)$ and $\beta_j(.)$ are holomorphic functions of ω across the whole considered gaps and such that*

$$\frac{\partial A}{\partial\omega} \le 0, \qquad \frac{\partial V}{\partial\omega} \ge 0, \qquad \frac{\partial\alpha_j}{\partial\omega} \ge 0, \qquad \frac{\partial\beta_j}{\partial\omega} \ge 0. \tag{37}$$

Then the conclusion of Lemma 4 holds: $\frac{dZ}{d\omega} < 0$. It follows that Theorems 1 and 2 are still valid.

Now we discuss three models involving (27) and (28). The first two models address the interface conditions α_j and β_j (28), while the third focuses on dispersive media with $A(x,\omega)$ and $V(x,\omega)$. In each case, an inner product (2) can be introduced to obtain a self-adjoint Hamiltonian. For model 1 and 3, we provide appropriate references.

5.3. Families of models

Model 1: imperfect contacts. As a first example, one considers usually $A(x,\omega) = E(x)$ and the bulk potential $V(x,\omega) = \rho(x)\,\omega^2$, whereas the interface parameters and the interface potentials write

$$\alpha_j = 1/K_j, \qquad \beta_j(\omega) = M_j\,\omega^2. \tag{38}$$

In (38), $K_j > 0$ and $M_j \geq 0$ are stiffness and mass terms. The mirror symmetry implies that $K_j = K_{N-j+1}$ $(j = 1, \cdots, N)$ and similarly for M_j. This model describes imperfect transmission of elastic waves through glue layers or cracks [33]. Conservation of energy is proven in [34]. The usual case of perfect contact is recovered when $K_j \to +\infty$ and $M_j = 0$. The inner product is defined in Appendix A of [33]. Since $\partial_\omega \beta_j = 2\, M_j\, \omega \geq 0$, the assumptions of Theorem 3 are satisfied.

Model 2: Helmholtz resonators. A second example concerns the propagation of acoustic waves in a waveguide connected with an array of Helmholtz resonators. This configuration is modelled by the Helmholtz equation (1) and the jump conditions

$$[\![p]\!]_{x_j} = 0, \qquad [\![v]\!]_{x_j} = \mathrm{i}\, g_j \, \frac{\omega^2}{\omega^2 - \omega_j^2}\, p(x_j), \tag{39}$$

where $v = -p'/(\mathrm{i}\,\omega\rho)$ is the acoustic velocity. The resonance frequencies ω_j and the coupling coefficients $g_j > 0$ are related with the geometry of the jth Helmholtz resonator. The jump conditions (39) can be replaced by (28) with

$$\alpha_j = 0, \qquad \beta_j = -g_j \, \frac{\omega^2}{\omega^2 - \omega_j^2}. \tag{40}$$

Since

$$\partial_\omega \beta_j(\omega) = 2\, g_j\, \omega_j^2 \, \frac{\omega}{\left(\omega^2 - \omega_j^2\right)^2} > 0, \tag{41}$$

the assumptions of Corollary 3 are satisfied except in gaps containing a resonance frequency. This argument can be used to prove rigorously the existence of topologically protected interface mode in a guide connected with a one-dimensional array of Helmholtz resonators [24, 25].

Model 3: dispersive media. As a third and last example, we consider acoustic dispersive media with null jump conditions ($\alpha_j = 0$ and $\beta_j = 0$ in (28)) but with frequency-dependent parameters:

$$\rho(x,\omega) = \rho_0(x) \left(1 - \frac{\Omega_\rho^2}{\omega^2 - \omega_\rho^2}\right), \qquad \kappa^{-1}(x,\omega) = \kappa_0^{-1}(x) \left(1 - \frac{\Omega_\kappa^2}{\omega^2 - \omega_\kappa^2}\right), \tag{42}$$

with $\rho_0(x) > 0$ and $\kappa_0(x) > 0$. Such parameters are generally obtained through an homogenization process. See [35] and references therein for application of (42) to acoustics in a guide with an array of Helmholtz resonators and membranes (model 2) in the low frequency range. In photonics, similar expressions hold for the permittivity and / or the permeability in the Drude-Lorentz model. Kramers-Kronig relations would involve additional imaginary parts $\mathrm{i}\gamma_\rho\omega$ and $\mathrm{i}\gamma_\kappa\omega$ in the pole of (42). However, these lossy terms are assumed to be small and are neglected here.

Injected in the acoustic Helmholtz equation (1), the parameters (42) lead to the potentials in (27) with

$$A(x,\omega) = \frac{1}{\rho(x,\omega)}, \qquad V(x,\omega) = \kappa^{-1}(x,\omega)\,\omega^2. \tag{43}$$

Since

$$\begin{aligned} \partial_\omega A &= -\frac{1}{\rho^2(x,\omega)}\partial_\omega \rho = -\frac{\rho_0(x)}{\rho^2(x,\omega)}\,\frac{\Omega_\rho^2\,\omega}{(\omega^2-\omega_\rho)^2} < 0, \\ \partial_\omega V &= 2\,\kappa_0^{-1}(x)\,\omega\left(1+\left(\frac{\Omega_\kappa\,\omega_\kappa}{\omega^2-\omega_\kappa^2}\right)^2\right) > 0, \end{aligned} \tag{44}$$

the conditions (37) in Corollary 3 are satisfied. The spectral properties of (27) for a general dispersive medium are analyzed in [30, 31]. The particular case of the Drude-Lorentz (42)-(43) is studied in [32] in the context of high-frequency homogenization. In the latter reference, it is shown that a spectrum accumulation point exists at the frequencies where $A(x,\omega) = 0$ or $V(x,\omega) = +\infty$. It occurs at $\sqrt{\omega_\rho^2+\Omega_\rho^2}$ or ω_κ. At the other frequencies, the coefficients of the dispersion relation are holomorphic. The roots of the dispersion relation are then isolated, ensuring the discrete nature of the spectrum. As a final remark, we notice that the generalization of (42) to multiple resonances is staightforward and yields a similar conclusion.

5.4. Numerical example: array of imperfect contacts

We now consider a configuration to illustrate the generalization presented previously (section 5). As we have shown in Theorem 3, we observe the presence of topological interface modes when the Zak phase differ on the left and right side of the interface, similarly to what we obtained for the bilayered model of section 4.5.

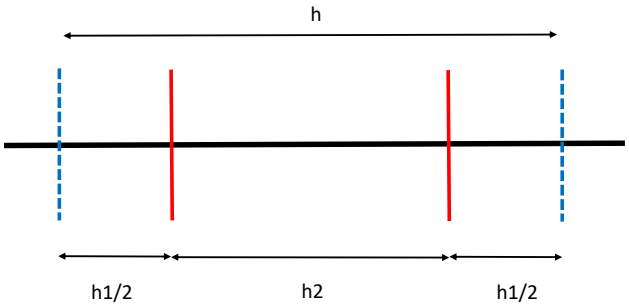

Figure 8: Elementary cell of a mirror symmetric PC. The red vertical solid lines denote the two interfaces with imperfect contacts. The blue vertical dotted lines denote the edges of the cell.

The model we consider contains two interfaces with imperfect contacts (28)-(38) of identical stiffness $Kh/E = 5.2$ and $M = 0$ (model 1 of section 5). The cell is mirror symmetric: the positions of the interfaces in the cell are denoted by $h_1 = \theta h$ and $h_2 = (1-\theta)h$, with $0 < \theta < 1$ (Figure 8). The transformation $\theta \mapsto 1-\theta$ yields a similar PC with identical gaps, contrary to the case of perfect contacts separating different media [17]. However, the symmetries of the

Bloch modes may differ, which will be useful for the construction of topologically protected interface modes.

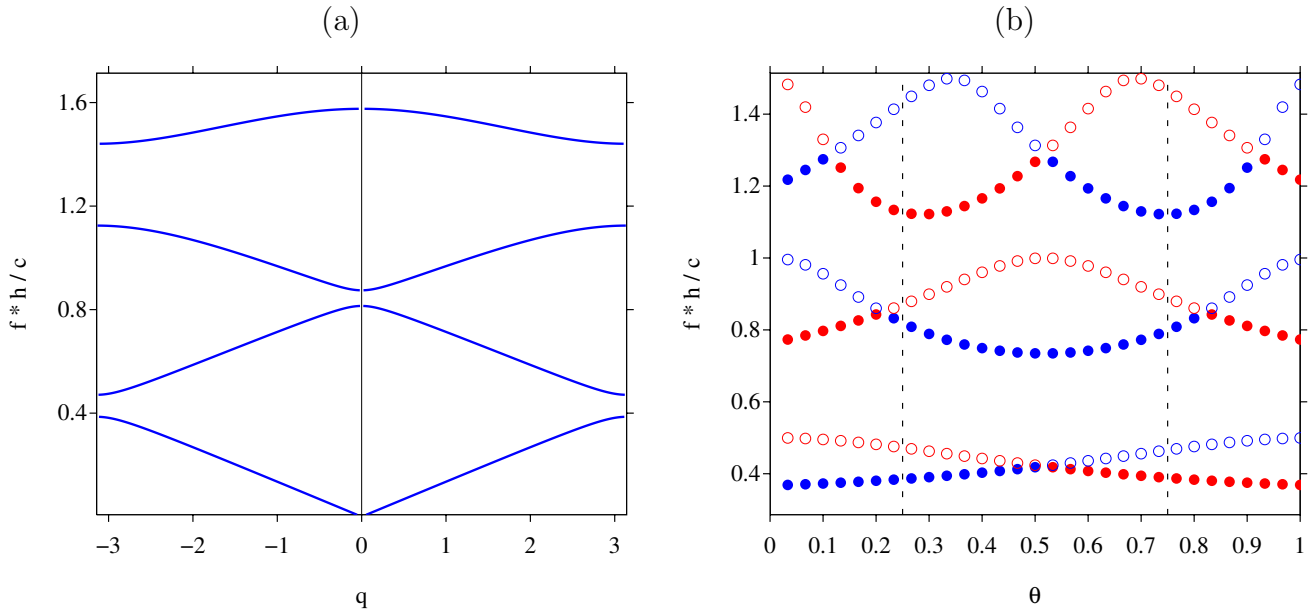

Figure 9: (a) Bloch-Floquet dispersion diagram in the case $\theta = 0.25$, with the Bloch shift $q = kh$, in scaled frequency (a). Parametric study of the Bloch modes at the band edges, in terms of θ (b). The full and empty circles denote the lower edge λ_n^+ and the upper edge λ_{n+1}^- of the gap Ω_n ($n = 1 \cdots 3$), respectively. The blue and red circles denote symmetric and antisymmetric Bloch modes, respectively. The vertical dotted lines denote $\theta = 0.25$ and $\theta = 0.75$.

Figure 9-(a) displays the Bloch-Floquet dispersion diagram in the case $\theta = 0.25$. The vertical axis shows the range of scaled frequencies $\tilde{f} = f \times h/c$. A similar scaling is used all along the text; notably, one denotes $\tilde{f}_n^{\pm} = \sqrt{\lambda_n^{\pm}}/(2\pi) \times h/c$. As stated in Lemma 1, the Bloch modes at these edges are either symmetric or antisymmetric. Figure 9-(b) displays a parametric study of the symmetries of Bloch modes at the band edges, in terms of θ. The lower frequency λ_n^+ and the upper frequency λ_{n+1}^- of the gaps Ω_n are denoted by full and empty circles, respectively. A blue circle represents a symmetric Bloch wave, whereas a red circle represents an antisymmetric Bloch wave. One notices the symmetry of the frequencies with respect to $\theta = 0.5$, induced by the invariance of the PC by the transformation $\theta \mapsto 1 - \theta$. However, the symmetries of Bloch modes may differ when comparing θ and $1 - \theta$.

From now on, we focus on two particular values of θ: 0.25 and 0.75. The PCs built using these values are named PC-L and PC-R, respectively. The intersections between the bands and the vertical dotted lines in Figure 9-(b) determine the symmetries of u_n at the band edges. For instance, u_1 at the lower edge $\tilde{f}_1^+ = 0.385$ of the gap Ω_1 is expected to be symmetric (at $\theta = 0.25$) and antisymmetric (at $\theta = 0.75$). Figure 10 displays these Bloch modes; Figure 10-(a) amounts to u_1 in Figure 1-(a). One observes the change of symmetry of u_1 between PC-L and PC-R at this band edge.

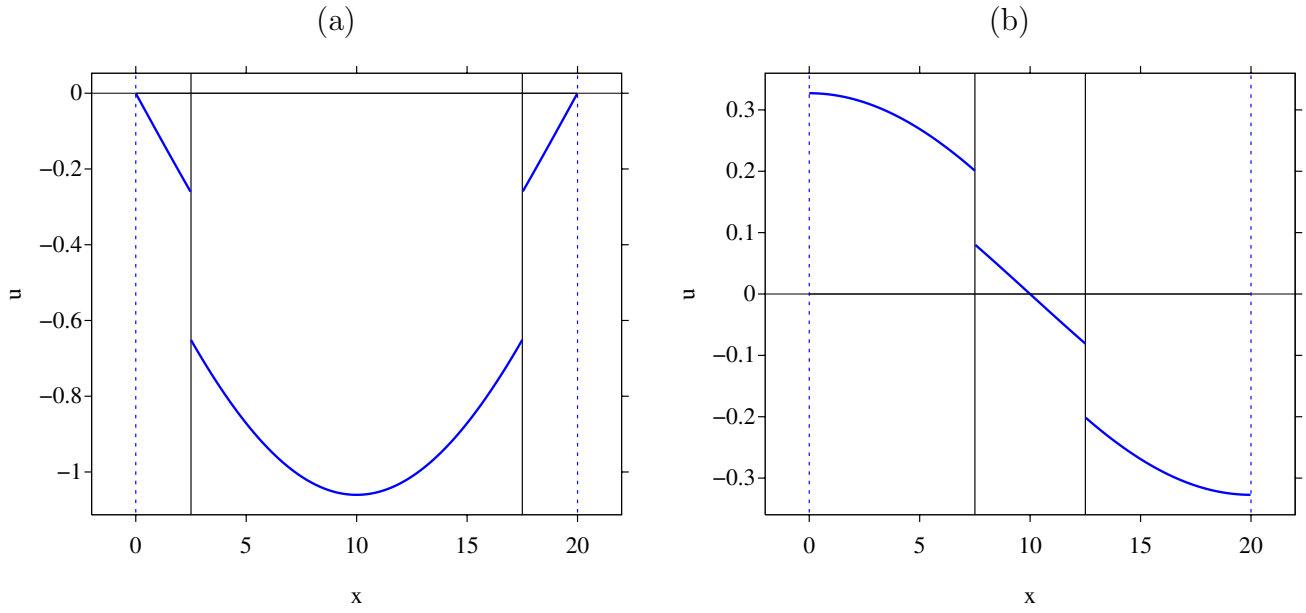

Figure 10: Bloch wave u_1 at the lower edge of gap Ω_1 ($\tilde{f}_1^+ = 0.385$). (a): $\theta = 0.25$, (b): $\theta = 0.75$. The vertical solid and dotted lines denote the interfaces and the edges of the elementary cell, respectively.

	$n=1$	$n=2$	$n=3$	$n=4$
$[\tilde{f}_n^+, \tilde{f}_{n+1}^-]$	[0.385, 0.470]	[0.814, 0.874]	[1.124, 1.440]	[1.575, 2.000]
PC-L	$\mathcal{S}$	$\mathcal{S}$	$\mathcal{A}$	$\mathcal{S}$
PC-R	$\mathcal{A}$	$\mathcal{S}$	$\mathcal{S}$	$\mathcal{S}$

Table 4: Scaled frequency intervals of the gaps Ω_n ($n = 1 \cdots 4$). Symmetries of the Bloch modes at scaled frequencies $\tilde{f}_n^+$, in PC-L ($\theta = 0.25$) and PC-R ($\theta = 0.75$).

The scaled frequencies and the symmetry of u_n at the band edges of Ω_n ($n = 1 \cdots 4$) are given in Table 4. Based on Theorem 1, we expect the existence of topologically protected interface modes in the gaps Ω_1 and Ω_3. On the contrary, no interface modes are expected in the gaps Ω_2 and Ω_4, where the symmetries of u_n are identical when $\theta = 0.25$ and $\theta = 0.75$. Now we glue PC-L and PC-R at $x = 0$ to illustrate this claim.

Figure 11 shows the frequency evolution of the surface impedance Z_L in PC-L, of the surface impedance Z_R in PC-R, and finally of their sum. In Figure 11-(a), we observe that $Z_L + Z_R = 0$ at $\tilde{f}_1^\sharp \approx 0.420$ in the gap Ω_1: according to Theorem 1, a topologically protected interface mode exists at this frequency. In Figure 11-(b,d), $Z_L + Z_R \neq 0$: no interface mode exists. In Figure 11-(c), $Z_L + Z_R = 0$ at $\tilde{f}_3^\sharp \approx 1.289$ in the gap Ω_3: once again, a topologically protected interface mode exists at this frequency.

Now, we look for the expected interface modes in a scattering configuration [37]. For this purpose, one considers finite PCs consisting of N cells with $\theta = 0.25$ on the left ($x < 0$), and N cells with $\theta = 0.75$ on the right ($x > 0$). Figure 12 shows the frequency evolution of the

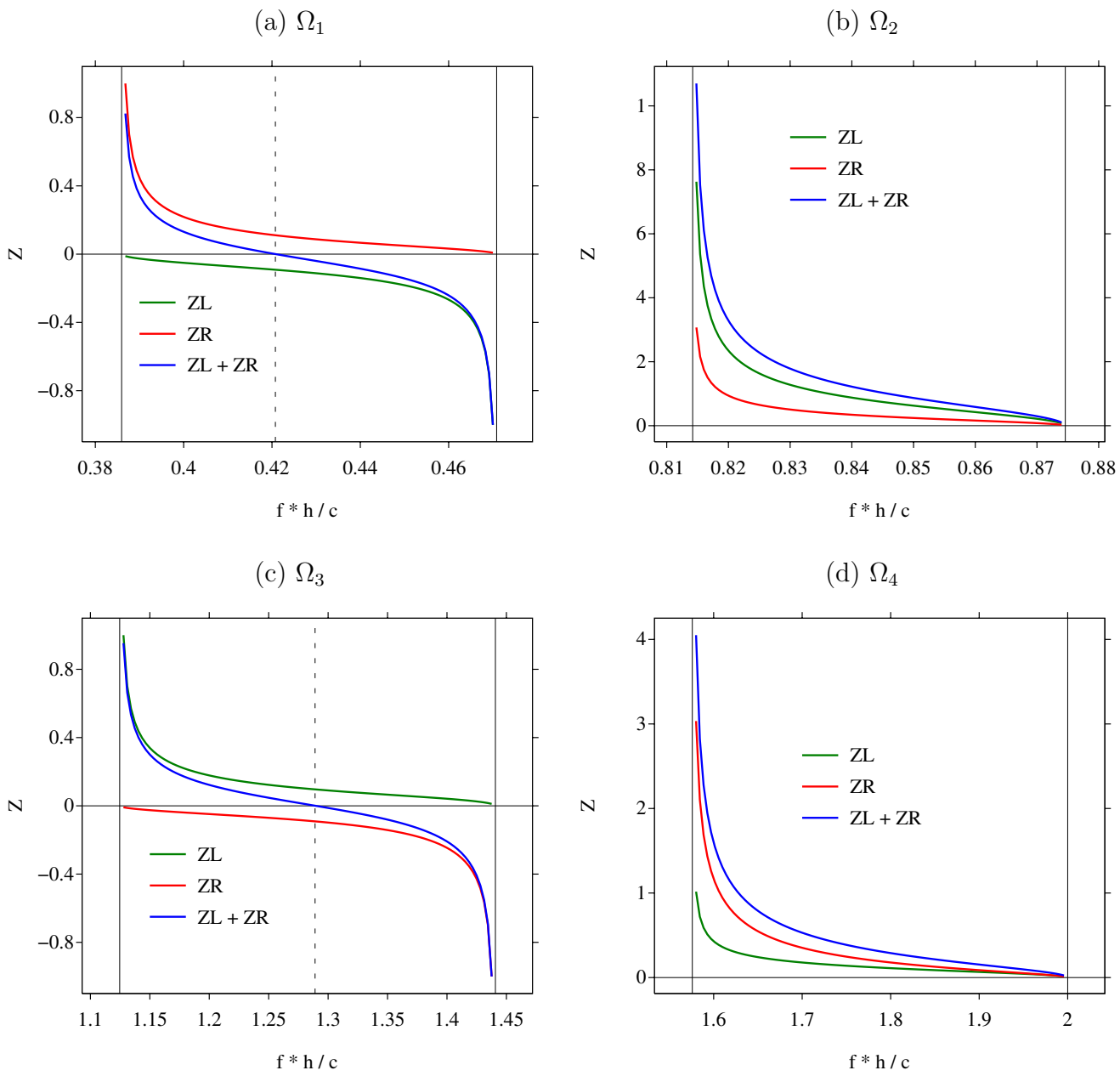

Figure 11: Frequency evolution of the surface impedances of the PCs in contact. The vertical solid lines denote the edges of the nth gap in scaled frequency. (a-c): gaps Ω_1 and Ω_3, in which a topologically protected interface mode exists. The vertical dotted line denotes the scaled frequency $\tilde{f}_1^\sharp \approx 0.42$ and $\tilde{f}_3^\sharp \approx 1.28$ where $Z_L + Z_R = 0$. (b-d): gaps Ω_2 and Ω_4, in which no topologically protected interface mode exists.

transmission coefficient through the slab of $2N$ cells, for $N = 3$ (a) and $N = 5$ (b). Successions of $N - 1$ equidistant oscillations are observed in the bands, corresponding to the modes of a cavity. More interestingly, isolated peaks are observed in the gaps Ω_1 (at $\tilde{f} \approx 0.420$) and Ω_3 (at $\tilde{f} = 1.289$). These scaled frequencies corresponds very accurately to the roots $\tilde{f}_1^\sharp$ and $\tilde{f}_3^\sharp$ of $Z_L + Z_R = 0$ observed in Figure 11-(a,c). As N increases, these peaks become thinner. In

12-(b), the peak in Ω_3 is so thin that the frequency discretization is insufficient to capture its spatial support.

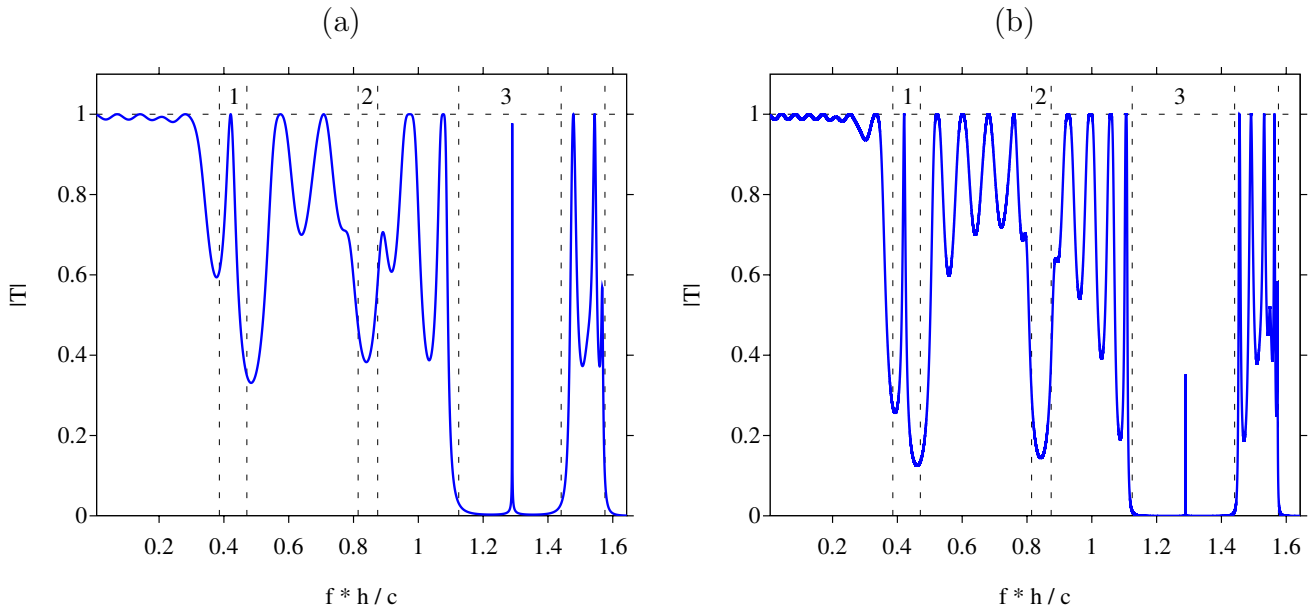

Figure 12: Modulus of the transmission coefficient in the case of $N = 3$ cells (a) and $N = 5$ cells (b) per PC. The vertical dashed lines denote the lower and upper edges of the gaps Ω_n ($n = 1 \cdots 3$), denoted by their numbering. An isolated peak is observed in the gaps Ω_1 and Ω_3.

Figure 13 represents the spatial evolution of the modulus of u at $\tilde{f}_1^\sharp$ and $\tilde{f}_3^\sharp$, with $N = 3$ cells in PC-L and PC-R. In both cases, an evanescent mode centered on the interface between the PCs is observed. It is a clear signature of an interface mode at the interface between PC-L and PC-R.

Finally, we study the evolution of the interface modes when the geometry of the elementary cell varies. The length h remains constant, but the parameter θ varies; the PC-R is built using the parameter $1 - \theta$. Figure 14 shows $\tilde{f}_1^\sharp$ (a) and $\tilde{f}_3^\sharp$ (b) as functions of θ. In (b), the minimum value of θ is 0.1; below this value, a Dirac point exists, as observed in the gap Ω_3 on Figure 1-(b). The blue lines denote the lower and upper edges of the gap Ω_1 (a) and Ω_3 (b). The red line denotes the scaled frequency of the interface mode, computed as the zero of $Z_L + Z_R$. At the scale of the Figure, this frequency seems contant when θ varies, which shows the robustness of the topologically protected interface modes. Nevertheless, a large zoom on the red line would show that $\tilde{f}_3^\sharp$ is not rigourously constant.

6. Conclusion

In this work, we considered semi-infinite PCs with mirror symmetry, which are joined together. To prove the existence of topologically protected interface modes in their common gaps, we used the concept of surface impedance. Initially introduced in [17] in the case of a bilayer

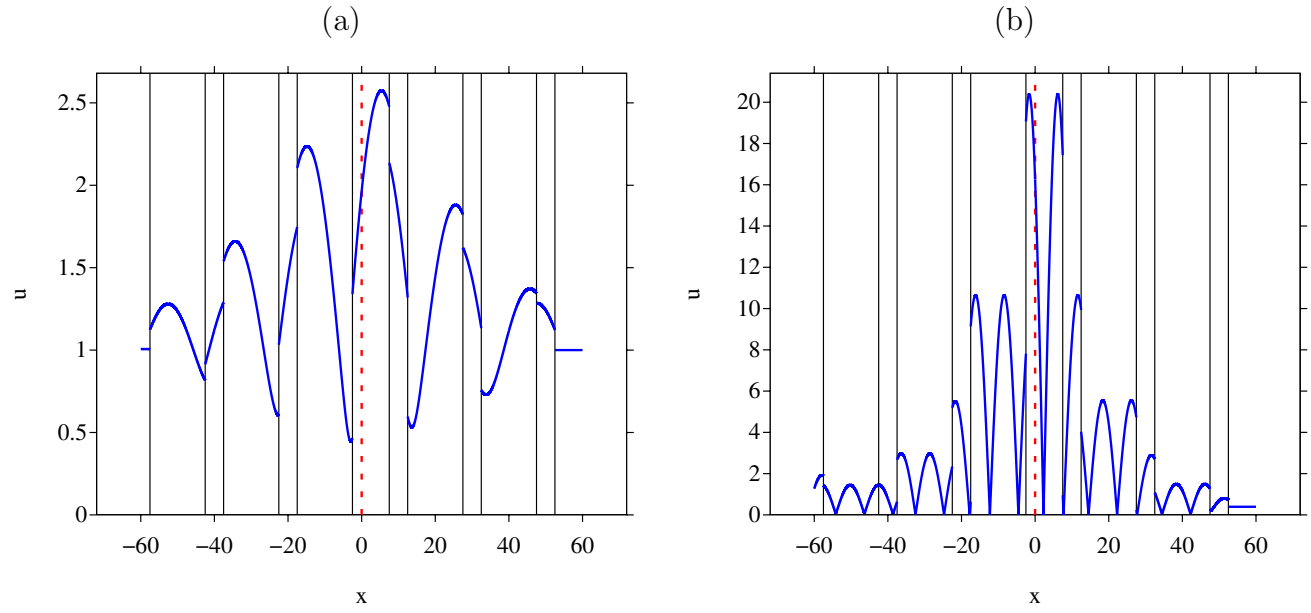

Figure 13: Spatial evolution of u at the scaled frequencies $\tilde{f}_1^\sharp = 0.420$ (a) and $\tilde{f}_3^\sharp = 1.289$. The vertical solid lines represent the interfaces with imperfect contacts. The red vertical dotted line at $x = 0$ denotes the interface between PC-L and PC-R, each being built with $N = 3$ cells.

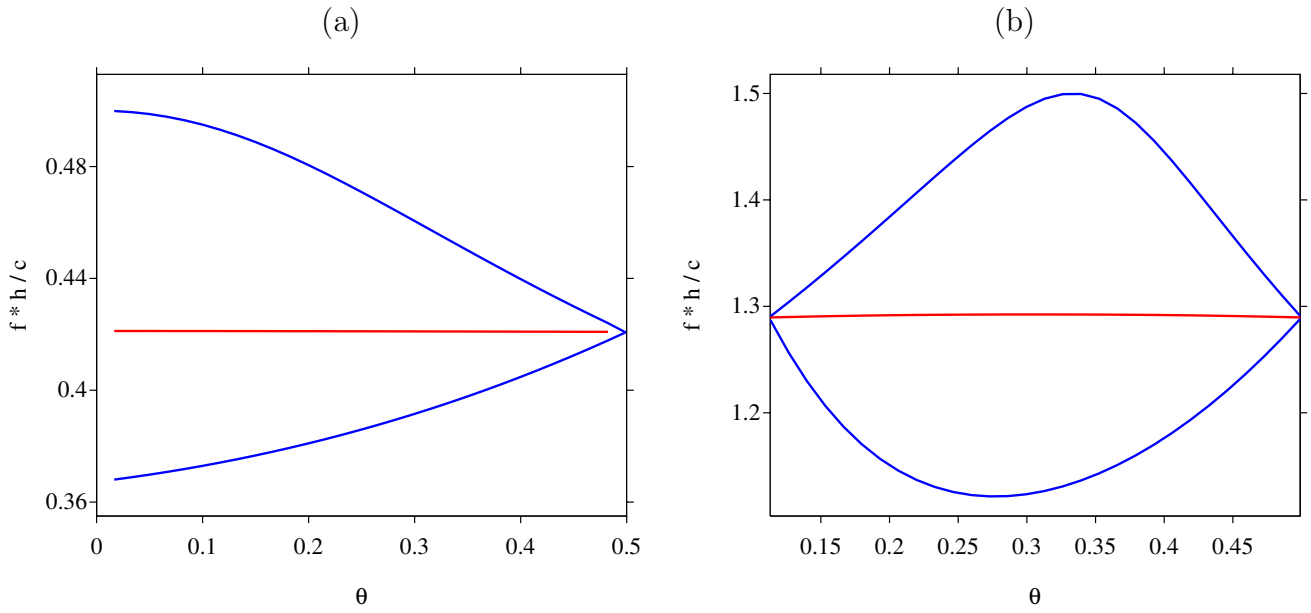

Figure 14: Frequency evolution of the topologically protected interface modes in the gaps Ω_1 (a) and Ω_3 (b), as a function of the parameter θ governing the geometry of the elementary cell. These scaled frequencies $\tilde{f}_1^\sharp$ (a) and $\tilde{f}_3^\sharp$ (b) are represented by a red line. The blue curves represent the scaled lower edge $\tilde{f}_n^+$ and scaled upper upper $\tilde{f}_{n+1}^-$ of the gaps Ω_n.

medium, we extended this approach to any mirror symmetric PC in 1D. The main result obtained in Theorem 1 states that a change of Zak phase, or equivalently a symmetry inversion

of Bloch modes at gap edges, guarantees the existence and unicity of topologically protected interface localized modes.

This work opens several research directions. The first natural extension would be the generalization of this approach to higher spatial dimensions. Zak phases have been used as topological indices in 2D systems characterizing the presence of edge waves [38, 39], but a relevant bulk-boundary correspondence has not been established so far [40]. Similarly, the concept of higher-order topological insulators have attracted a lot of attention in the recent years [41, 42]. For instance, 2D higher order topological insulators can host localized modes in their corners. Again, a complete understanding of the a higher-order bulk-boundary correspondence is still lacking, but the similarity with the present problem suggests that similar techniques might lead to progresses in that direction. Indeed, the study of 2D photonic surface modes from surface impedances was carried out for instance in [43], but so far without the prism of topology.

A simpler generalization of the present work would be to extend the proof to quasi-1D regimes. This work and previous ones [44, 17, 20, 21, 16] heavily rely on having only two modes at a given frequency (equation (1) is second order in space). It is an open question how to extend this to multimodal systems, such as finite width waveguide [45], or dispersive media containing higher-order spatial derivatives, such as flexural beams [46].

Another interesting research direction would be the investigation of topological modes in nonlinear regimes. In [47], the emergence of a topological mode in a discrete system alternating different nonlinear springs is shown, depending on the amplitude of the perturbations. The study of nonlinear topological modes in a continuous medium remains a open subject. Let us note that the imperfect conditions (28) easily allow the introduction of nonlinear mechanisms [34].

Finally, we have considered lossless media here, which simplifies the spectral structure. It would be interesting to generalize the analysis of topological modes by surface impedance to the case of dissipative media.

Acknowledgements. We thank one of the Reviewers for drawing our attention to the spectral properties of dispersive media (Section 5). Clarifications on this point have resulted from very interesting discussions with Marie Touboul and Raphaël Assier, who are hereby warmly thanked. We also thank Guillaume Demesy for suggestion of a generalization.

Note added. After we submitted this manuscript, we became aware of reference [18], which reaches similar conclusions. In particular, the monotonicity of the impedance with frequency is also shown, although restricted to the Helmholtz equation (1) and not the generalization of equation (27).

Appendix A. Zak phase as a topological invariant

In this appendix, we show how to relate the Zak phase with the symmetries of the Bloch modes on the band edges. To ease the discussion, we start by recalling the definition of the Berry connection in equation (9):

$$A_n(q) = -\mathrm{i}\,\langle u_n(q)|\partial_q u_n(q)\rangle\,. \tag{A.1}$$

The Berry connection in (A.1) is defined up to a gauge transformation. Indeed, one can always redefine the Bloch modes by changing its phase, as

$$\tilde{u}_n(q) = e^{\mathrm{i}\theta(q)} u_n(q). \tag{A.2}$$

Assuming that θ is a smooth function of q, this gives the new connection

$$\tilde{A}_n(q) = A_n(q) + \frac{d\theta}{dq}. \tag{A.3}$$

Remembering that the Zak phase is obtained as the integral of the Berry connection over the Brillouin zone, as defined in equation (10), the latter can be computed with either connection. The gauge transformation (A.3) shows that:

$$\int_{-\pi}^{\pi} \tilde{A}_n(q)dq = \int_{-\pi}^{\pi} A_n(q)dq + \theta(\pi) - \theta(0). \tag{A.4}$$

Since $e^{\mathrm{i}\theta(q)}$ must be 2π-periodic, $\theta(\pi) - \theta(0)$ is a multiple of 2π. This shows that the Zak phase modulo 2π is a gauge invariant quantity (i.e. independent of a particular choice of Bloch mode basis). At this level, it is worth noting that the Berry connection is defined here using Bloch modes satisfying the Bloch condition $u_q(x+h) = e^{\mathrm{i}q}u_q(x)$ (see equation (4)). The advantage is that u_q is periodic in q, and hence, the proof of gauge invariance follows naturally, as we just saw. An alternative definition is sometimes found in the literature [48], which uses the periodic part of u_q:

$$\psi_q(x) = e^{-\mathrm{i}qx/h} u_q(x). \tag{A.5}$$

While $\psi_q(x)$ is periodic in x, it is no longer in q, and hence, the gauge invariance of the Zak phase defined in this manner is quite cumbersome. [1]

Moreover, when the system is mirror symmetric, the connection at q can be related to that at $-q$. Indeed, by taking the derivative of equation (6) with respect to q, and the scalar product with $u_n(-q)$ we obtain:

$$A_n(-q) = A_n(q) + \partial_q \xi_n. \tag{A.6}$$

[1] In fact, the original paper by Zak uses the latter choice, and hence contains a lengthy discussion about gauge invariance.

In other words, the Berry connection at q differs from that at $-q$ by a total derivative. Now, if we integrate this relation over half of the Brillouin zone, we obtain

$$-\int_{-\pi}^{0} A_n(q)dq = \int_{0}^{\pi} A_n(q)dq + \xi_n(\pi) - \xi_n(0). \tag{A.7}$$

Combining the two integrals gives the integral over the whole Brillouin zone, and hence, the identity (11) for the Zak phase. We can also notice that for mirror symmetric systems, the Zak phase defined using the spatially periodic modes $\psi_q(x)$ differs by π. More precisely, by inspecting equation (A.5) and using the expression (11), we see that the Zak phase computed with ψ_q is 0 when Φ_n is π, and *vice-versa*. Importantly, while the value of the Zak phase differ, the change of topological phase between two system is identical whether one uses u_q of ψ_q.

Appendix B. Transfer matrix

Alternative proofs can be obtained through the usual transfer matrix. Here we list some useful results. Setting

$$\mathbf{U}(x,\omega) = \begin{pmatrix} u \\ E\,u' \end{pmatrix}, \qquad \mathbf{A}(x,\omega) = \begin{pmatrix} 0 & 1/E(x) \\ -\rho(x)\,\omega^2 & 0 \end{pmatrix}, \tag{B.1}$$

then the Helmholtz equation (1) writes as a differential equation on $[0,h]$

$$\frac{d}{dx}\mathbf{U} = \mathbf{A}\,\mathbf{U}, \qquad x \notin \mathcal{I}, \tag{B.2}$$

where $\mathcal{I} = \{x_i, \cdots, x_N\}$ is the set of interfaces on a elementary cell. The generalizations described in Section 5 can be included in this formalism; in particular, the case of dispersive media is described by considering frequency-dependent physical parameters in (B.1). Integration of (B.2) on the subintervals $]x_j, x_{j+1}[$ and use of the jump conditions lead to

$$\mathbf{U}(h,\omega) = \mathbf{M}\,\mathbf{U}(0,\omega), \tag{B.3}$$

where $\mathbf{M}$ is the transfer matrix in $\mathcal{M}_2(\mathbb{R})$. Reciprocity and conservation of energy yields the general form

$$\mathbf{M}(\omega) = \begin{pmatrix} \alpha(\omega) & \beta(\omega) \\ \tilde{\beta}(\omega) & \alpha(\omega) \end{pmatrix}, \qquad \det(\mathbf{M}) = 1. \tag{B.4}$$

Bloch-Floquet theorem implies that $\mathbf{U}(h,\omega) = \Lambda\,\mathbf{U}(0,\omega)$ with $\Lambda = e^{\mathrm{i}q}$, where $q \in [0, \pm\pi]$ is the Bloch wavenumber. Comparison with (B.3) gives that $\Lambda := \Lambda_{0,1}$ are the eigenvalues of $\mathbf{M}$. One also obtains the relations

$$\Lambda_0 + \Lambda_1 = 2\alpha \in \mathbb{R}, \qquad \Lambda_0\,\Lambda_1 = \alpha^2 - \beta\tilde{\beta} = 1. \tag{B.5}$$

Depending on ω, two cases occur. In the first case $|\Lambda_{0,1}| = 1$, the eigenvalues are complex conjugate, hence $q_{0,1}$ is purely real: it corresponds to a band. In the second case $|\Lambda_{0,1}| \neq 1$, the eigenvalues are real and have the same sign, hence $q_{0,1}$ is purely imaginary: it corresponds to a gap. Some useful results on the coefficients of $\mathbf{M}$ are now stated.

Lemma 5 (Coefficient α)**.** *The following properties hold:*

- *in bands:* $|\alpha(\omega)| < 1$*;*
- *in gaps:* $|\alpha(\omega)| > 1$*;*
- *on the edges of gaps:* $|\alpha(\omega)| = 1$*.*

Proof. In a band, $\Lambda_{0,1}$ are complex conjugates. From (B.5), it follows that $\alpha = \Re\mathrm{e}(\Lambda_0) \in]0,1[$, and hence $|\alpha| < 1$. In a gap at $q = 0$, then $\Lambda_0 = y \in]0,1[$ and $\Lambda_1 = 1/y$. It follows $\alpha = (y + 1/y)/2$ and $\frac{\mathrm{d}\alpha}{\mathrm{d}y} = (1 - 1/y^2)/2 < 0$. Since $\alpha = 1$ when $y = 1$, then $\alpha > 1$ for all $y < 1$. The same argument holds in a gap at $q = \pi$. Lastly, at the band edges one has $\Lambda_0 = \Lambda_1 = \pm 1$, which concludes the proof. □

Lemma 6 (Coefficients β and $\tilde{\beta}$)**.** *The following properties hold:*

- *in bands,* $\beta(\omega)$ *and* $\tilde{\beta}(\omega)$ *have opposite signs;*
- *in gaps,* $\beta(\omega)$ *and* $\tilde{\beta}(\omega)$ *have the same sign;*
- $\beta(\omega)$ *or* $\tilde{\beta}(\omega)$ *vanishes at edges of gaps.*

Proof. From (B.5), it follows $\beta\,\tilde{\beta} = \alpha^2 - 1$. The different cases in Lemma 5 allow to conclude. □

From these results on the coefficients of $\mathbf{M}$, we obtain an alternative proof of Lemma 2 without using the property of interlacing (8).

Lemma 7 (Inversion of parity)**.** *Let us consider a mirror symmetric PC, where the* j*th band is isolated. Then the Bloch modes on each edge of the gap* $[\lambda_j^+, \lambda_{j+1}^-]$ *attain different symmetries.*

Proof. The impedance Z reaches $\pm\infty$ or 0 at the edge of the gap and is a strictly decreasing function of ω (Lemma 4 and Table 2). There are then 3 cases: i) $Z(\lambda_j^+) = +\infty$ and $Z(\lambda_{j+1}^-) = 0$; ii) $Z(\lambda_j^+) = 0$ and $Z(\lambda_{j+1}^-) = -\infty$; iii) $Z(\lambda_j^+) = +\infty$ and $Z(\lambda_{j+1}^-) = -\infty$. In cases i) and ii), there is a symmetry inversion of the Bloch mode. Let's show that case iii) is impossible.

From (B.4), the components of the eigenvector $\mathbf{U}(0)$ of $\mathbf{M}$ satisfy

$$\begin{cases} \beta\, E\, u'(0,\omega) = (\Lambda - \alpha)\, u(0,\omega), \\ \tilde{\beta} u(0,\omega) = (\Lambda - \alpha)\, E\, u'(0,\omega), \end{cases}$$

and hence

$$Z(\omega) = \frac{\beta(\omega)}{\Lambda(\omega) - \alpha(\omega)}.$$

In gaps, Lemmas 5 and 6 give $\alpha(\omega) \neq \Lambda(\omega)$ and $\beta(\omega) \neq 0$. It implies that the surface impedance is real, finite, and never vanishes. Since Z is continuous, this implies that case iii) is impossible.

Hence, $Z(\omega)$ is $\pm\infty$ on one edge of the gap, and vanishes on the other edge. Using Table 2, this means that either the symmetry of the Bloch modes are changed, or the value of the Bloch wavenumber changes. However, the latter is impossible by the continuity of the function $\omega \mapsto \alpha(\omega)$ (it is holomorphic). Indeed, if the gap starts at $q = 0$ (i.e. $\alpha = 1$), then $\alpha(\omega) > 1$ in that gap. By continuity, the gap must end again at $q = 0$ ($\alpha = 1$). The same follows for a gap starting at $q = \pi$ (i.e. $\alpha = -1$), which must end at $q = \pi$. This concludes the proof of Lemma 7. □

Appendix C. Jump of the Wronskian across an imperfect interface

The following Lemma used in Section 5.2 is introduced.

Lemma 8. *Let x_j be an interface with jump conditions (28). Then the jump of the Wronskian (19) across x_j satisfies*

$$\llbracket \mathcal{W} \rrbracket_{x_j} = \partial_\omega \alpha_j \langle A\, u' \rangle_{x_j}^2 + \partial_\omega \beta_j \langle u \rangle_{x_j}^2 + \llbracket \partial_\omega A\, u\, u' \rrbracket_{x_j} . \tag{C.1}$$

Proof. Let $\varphi = \partial_\omega u$. For any two functions f and g, the following identity (that can be proved directly) is valid:

$$\llbracket f g \rrbracket_{x_j} = \llbracket f \rrbracket_{x_j} \langle g \rangle_{x_j} + \langle f \rangle_{x_j} \llbracket g \rrbracket_{x_j} . \tag{C.2}$$

Differentiating (28) with respect to ω yields

$$\begin{aligned} &\llbracket \varphi \rrbracket_{x_j} = \partial_\omega \alpha_j \langle A\, u' \rangle_{x_j} + \alpha_j \langle \partial_\omega A\, u' \rangle_{x_j} + \alpha_j \langle A\, \varphi' \rangle_{x_j} , \\ &\llbracket \partial_\omega A\, u' \rrbracket_{x_j} + \llbracket A\, \varphi' \rrbracket_{x_j} = -\partial_\omega \beta_j \langle u \rangle_{x_j} - \beta_j \langle \varphi \rangle_{x_j} . \end{aligned} \tag{C.3}$$

Using (19), (C.2) and (C.3) leads to

$$\begin{aligned} \llbracket \mathcal{W} \rrbracket_{x_j} &= \llbracket \varphi\, A\, u' \rrbracket_{x_j} - \llbracket u\, A\, \varphi' \rrbracket_{x_j} , \\ &= \llbracket \varphi \rrbracket_{x_j} \langle A\, u' \rangle_{x_j} + \langle \varphi \rangle_{x_j} \llbracket A\, u' \rrbracket_{x_j} - \llbracket u \rrbracket_{x_j} \langle A\, \varphi' \rangle_{x_j} - \langle u \rangle_{x_j} \llbracket A\, \varphi' \rrbracket_{x_j} , \\ &= \partial_\omega \alpha_j \langle A\, u' \rangle_{x_j}^2 + \partial_\omega \beta_j \langle u \rangle_{x_j}^2 + \alpha_j \langle A\, u' \rangle_{x_j} \langle \partial_\omega A\, u' \rangle_{x_j} + \llbracket \partial_\omega A\, u' \rrbracket_{x_j} \langle u \rangle_{x_j} , \\ &= \partial_\omega \alpha_j \langle A\, u' \rangle_{x_j}^2 + \partial_\omega \beta_j \langle u \rangle_{x_j}^2 + \llbracket u \rrbracket_{x_j} \langle \partial_\omega A\, u' \rangle_{x_j} + \llbracket \partial_\omega A\, u' \rrbracket_{x_j} \langle u \rangle_{x_j} . \end{aligned} \tag{C.4}$$

Applying the identity (C.2) to the last two terms concludes the proof. □

[1] Ashcroft N W and Mermin N D. 1976 *Solid state physics*, Brooks Cole, USA.

[2] Joannopoulos J D, Johnson S G, Winn J N, and Meade R D. 2008 *Photonic Crystals: Molding the Flow of Light*, Princet. Univ. Press. Princeton.

[3] Laude V. 2020 *Phononic Crystals: Artificial Crystals for Sonic, Acoustic, and Elastic Waves*, Walter de Gruyter GmbH & Co KG.

[4] Reed M and Simon B. 1978 *Methods of Modern Mathematical Physics. IV. Analysis of Operators*, vol. 4. Academic Press.

[5] Allaire G and Capdeboscq Y. 2002 *Homogenization and localization for a 1-d eigenvalue problem in a periodic medium with an interface*, Annali di Matematica Pura ed Applicata **181**, 247–282.

[6] Ozawa T, Price H M, Amo A, Goldman N, Hafezi M, Lu L, Rechtsman M C, Schuster D, Simon J, Zilberberg O, et al.. 2019 *Topological photonics*, Reviews of Modern Physics **91-1**, 015006.

[7] Ma G, Xiao M, and Chan CT. 2019 *Topological phases in acoustic and mechanical systems*, Nature Reviews Physics **1-4**, 281–294.

[8] Asbóth JK, Oroszlány L, and Pályi A. 2019 *A short course on topological insulators*, Lecture Notes in Physics **919**, 87.

[9] Prodan E and Schulz-Baldes H. 2016 *Bulk and Boundary Invariants for Complex Topological Insulators*, Springer, Cham.

[10] Delplace P, Ullmo D, and Montambaux G. 2011 *Zak phase and the existence of edge states in graphene*, Phys. Rev. **84-B** 19, 195452.

[11] Delplace P. 2021 *Berry-Chern monopoles and spectral flows.*

[12] Hatsugai Y. 1993 *Chern number and edge states in the integer quantum hall effect*, Phys. Rev. Lett. **71**, 3697–3700.

[13] Essin AM and Gurarie V. 2011 *Bulk-boundary correspondence of topological insulators from their respective Green's functions*, Phys. Rev. B **84**, 125132.

[14] Zak J. 1989 *Berry's phase for energy bands in solids*, Phys. Rev. Lett. **62**, 2747–2750.

[15] Fefferman C and Weinstein M. 2012 *Honeycomb lattice potentials and Dirac points*, Journal of the American Mathematical Society **25-4**, 1169–1220.

[16] Lin J and Zhang H. 2022 *Mathematical theory for topological photonic materials in one dimension*, Journal of Physics A: Mathematical and Theoretical **55-49**, 495203.

[17] Xiao M, Zhang Z, and Chan CT. 2014 *Surface impedance and bulk band geometric phases in one-dimensional systems*, Phys. Rev. X **4-2**, 021017.

[18] Thiang GC, and Zhang H. 2023 *Bulk-interface correspondences for one-dimensional topological materials with inversion symmetry*, Proceedings of the Royal Society A **479-2270**, 20220675.

[19] Tsukerman I and Markel V. 2023 *Topological features of Bloch impedance*, Europhysics Letters **144-1**, 16002.

[20] Gontier D. 2020 *Edge states in ordinary differential equations for dislocations*, Journal of Mathematical Physics **61-4**.

[21] Drouot A. 2021 *The bulk-edge correspondence for continuous dislocated systems*, Annales de l'Institut Fourier **71-3**, 1185–1239.

[22] Su WP, Schrieffer JR, Heeger AJ. 1979 *Solitons in Polyacetylene*, Physical Review Letters **42-25**, 16981701.

[23] Coutant A, Sivadon A, Zheng L, Achilleos V, Richoux O, Theocharis G, and Pagneux V. 2021*Acoustic Su-Schrieffer-Heeger lattice: Direct mapping of acoustic waveguides to the Su-Schrieffer-Heeger model*, Phys. Rev. B **103-22**.

[24] Zhao D, Chen X, Li P, and Zhu XF. 2021 *Subwavelength acoustic energy harvesting via topological interface states in 1d Helmholtz resonator arrays*, AIP Advances **11-1**, 015241.

[25] Li ZW, Fang XS, Liang B, Li Y, and Cheng JC. 2020 *Topological interface states in the low-frequency band gap of one-dimensional phononic crystals*, Physical Review Applied **14-5**, 054028.

[26] Kuchment PA. 1993 *Floquet Theory for Partial Differential Equations*, 60, Springer Science & Business Media.

[27] Brown BM, Eastham MS, and Schmidt KM. 2012 *Periodic Differential Operators*, 228 Springer Science & Business Media.

[28] Shahraki DP and Guzina BB. 2022 *From d'Alembert to Bloch and back: A semi-analytical solution of 1d boundary value problems governed by the wave equation in periodic media*, International Journal of Solids and Structures **234-235**, 111239.

[29] Weidmann J. 2006 *Spectral Theory of Ordinary Differential Operators*, 1258. Springer.

[30] Combes JM, Gralak B, and Tip A. 2002 *Spectral properties of absorptive photonic crystals*, Waves in Periodic and Random Media, Contemporary Mathematics **339**.

[31] Engström C and Richter M. 2009 *On the spectrum of an operator pencil with applications to wave propagation in periodic and frequency dependent materials*, SIAM Journal on Applied Mathematics **70-1**, 231247.

[32] Touboul M, Vial B, Assier R, Guenneau S, Craster R. 2023 *High-frequency homogenization for periodic dispersive systems*, arXiv:2308.08559 [physics.class-ph].

[33] Assier R, Touboul M, Lombard B, and Bellis C. 2020 *High-frequency homogenization in periodic media with imperfect interfaces*, Proceedings of the Royal Society A **476-2244**, 20200402.

[34] Bellis C, Lombard B, Touboul M, and Assier R. 2021 *Effective dynamics for low-amplitude transient elastic waves in a 1d periodic array of non-linear interfaces*, Journal of the Mechanics and Physics of Solids **149**, 104321.

[35] Bellis C and Lombard B. 2019 *Simulating transient wave phenomena in acoustic metamaterials using auxiliary fields*, Wave Motion **86**, 175–194.

[36] Cassier M, Joly P, and Kachanovska M. 2017 *Mathematical models for dispersive electromagnetic waves: an overview*, Computers & Mathematics with Applications, 74-11, 2792–2830.

[37] Kalozoumis PA, Theocharis G, Achilleos V, Félix S, Richoux O, and Pagneux V. 2018 *Finite-size effects on topological interface states in one-dimensional scattering systems*, Phys. Rev. A **98**, 023838.

[38] Liu F and Wakabayashi K. 2017 *Novel topological phase with a zero Berry curvature*, Phys. Rev. Lett. **118-7**, 076803.

[39] Liu F, Yamamoto M, and Wakabayashi K. 2017 *Topological edge states of honeycomb lattices with zero Berry curvature*, Journal of the Physical Society of Japan **86-12**, 123707.

[40] Xu S, Wang Y, and Agarwal R. 2023 *Absence of topological protection of the interface states in Z2 photonic crystals*, ArXiv:2303.12617.

[41] Schindler F, Cook AM, Vergniory MG, Wang Z, Parkin SS, Bernevig BA, and Neupert T. 2018 *Higher-order topological insulators*, Science Advances **4-6**, eaat0346.

[42] Benalcazar WA, Bernevig BA, and Hughes TL. 2017 *Quantized electric multipole insulators*, Science **357-6346**, 61–66.

[43] Lawrence FJ, Botten LC, Dossou KB, McPhedran R, and de Sterke CM. 2010 *Photonic-crystal surface modes found from impedances*, Physical Review A **82-5**, 053840.

[44] Fefferman CL, Lee-Thorp JP, and Weinstein MI. 2014 *Topologically protected states in one-dimensional continuous systems and Dirac points*, Proceedings of the National Academy of Sciences **111-24**, 8759–8763.

[45] Pagneux V, Amir N, and Kergomard J. 1996 *A study of wave propagation in varying cross-section waveguides by modal decomposition. Part I. Theory and validation*, The Journal of the Acoustical Society of America **100-4**, 2034–2048.

[46] Carta G and Brun M. 2015 *Bloch–Floquet waves in flexural systems with continuous and discrete elements*, Mechanics of Materials **87**, 11–26.

[47] Chaunsali R and Theocharis G. 2019 *Self-induced topological transition in phononic crystals by nonlinearity management*, Phys. Rev. B **100**, 014302.

[48] Cayssol J and Fuchs JN. 2021 *Topological and geometrical aspects of band theory*, Journal of Physics: Materials **4-3**, 034007.